Article

Not peer-reviewed version

# Slc11 Synapomorphy: A Conserved 3D Framework Articulating Carrier Conformation Switch

Mathieu FM Cellier *

Posted Date: 18 August 2023

doi: 10.20944/preprints202308.1317.v1

Keywords: AF2-CF modeling; LeuT fold; Slc11 synapomorphy; carrier conformation switch; phylogenetic analysis; in silico mutagenesis; epistasis

*Article*

# Slc11 Synapomorphy: A Conserved 3D Framework Articulating Carrier Conformation Switch

**Mathieu FM Cellier**

INRS-Centre Armand-Frappier Santé Biotechnologie, Laval, Québec; mathieu.cellier@inrs.ca

**Abstract:** Transmembrane carriers of the Slc11 family catalyze proton ($H^+$)-dependent uptake of divalent metal-ions ($Me^{2+}$) such as manganese and iron - vital elements coveted during infection. Slc11 mechanism of high affinity $Me^{2+}$ cell import is selective and conserved between prokaryotic (MntH) and eukaryotic (Nramp) homologs, though processes coupling the use of the proton motive force to $Me^{2+}$ uptake evolved repeatedly. Adding bacterial piracy of *Nramp* genes spread in distinct environmental niches suggests selective gain of function that may benefit opportunistic pathogens. To better understand Slc11 evolution Alphafold (AF2)/Colabfold (CF) 3D predictions for bacterial sequences from sister clades of eukaryotic descent (MCb and MCg) were compared using both native and mutant templates. AF2/CF model an array of native MCb intermediates spanning the transition from outward open (OO) to inward open (IO) carrier. In silico mutagenesis targeting i) a set of (evolutionary coupled) sites that may define Slc11 function (putative synapomorphy), and ii) residues from networked communities evolving during MCb transition, indicate Slc11 synapomorphy primarily instructs $Me^{2+}$-selective conformation switch which unlocks carrier inner gate, and contributes to $Me^{2+}$ binding site occlusion and outer gate locking. Inner gate opening apparently proceeds from interaction between transmembrane helix (h) h5, h8 and h1a. MCg1 xenologs revealed marked differences in carrier shape and plasticity, owing partly to altered intramolecular $H^+$-network. Yet, targeting Slc11 synapomorphy also converted MCg1 IO models to OO state, apparently mobilizing the same residues to control gates. But MCg1 response to mutagenesis differed, extensive divergence within this clade correlating with MCb-like modeling properties. Notably, MCg1 divergent epistasis marks emergence of the genus *Bordetella-Achromobacter*. Slc11 synapomorphy localizes to the 3D areas that deviate least among MCb and MCg1 models (either IO or OO) implying it constitutes a 3D network of residues articulating $Me^{2+}$-selective carrier conformation switch which is maintained in fast evolving clades at the cost of divergent epistatic interactions impacting carrier shape and dynamics.

**Keywords:** AF2-CF modeling; LeuT fold; Slc11 synapomorphy; carrier conformation switch; phylogenetic analysis; in silico mutagenesis; epistasis

## 1. Introduction

The physiological hallmark of transmembrane carriers of the Slc11 family is to catalyze $H^+$-dependent, high affinity import of $Me^{2+}$ such as manganese (Mn) and ferrous iron (Fe) into the cytoplasm [1,2]. Slc11 carriers use a chemiosmotic mechanism of transport rooted deep in their evolutionary history, the 'rocking bundle' (or 'gated channel') mechanism [3] that was discovered after solving structures of the LeuT-fold [4], and which may be declined in as many versions as diverse families form the superfamily APC (PFAM Clan CL0062) [5]. Among these, PFAM family 1566 comprises both the Slc11 family and phylogenetic outgroups (orphan- and NRMT-types) [6–8], which diverged specifically at the $Me^{2+}$ substrate binding site ($Me^{2+}$ BS) plus several sites that together remained (quasi-) invariant in Slc11 carriers. These sites constitute type ii evolutionary rate-shifts [9] and their co-occurrence is hereafter referred to as 'Slc11 synapomorphy' [10,11]. As such, Slc11 basic mechanism of high affinity $Me^{2+}$ cell import is considered family-specific and evolutionary conserved (Figure 1, left panel).

Preprints (www.preprints.org) | NOT PEER-REVIEWED | Posted: 18 August 2023 doi:10.20944/preprints202308.1317.v1



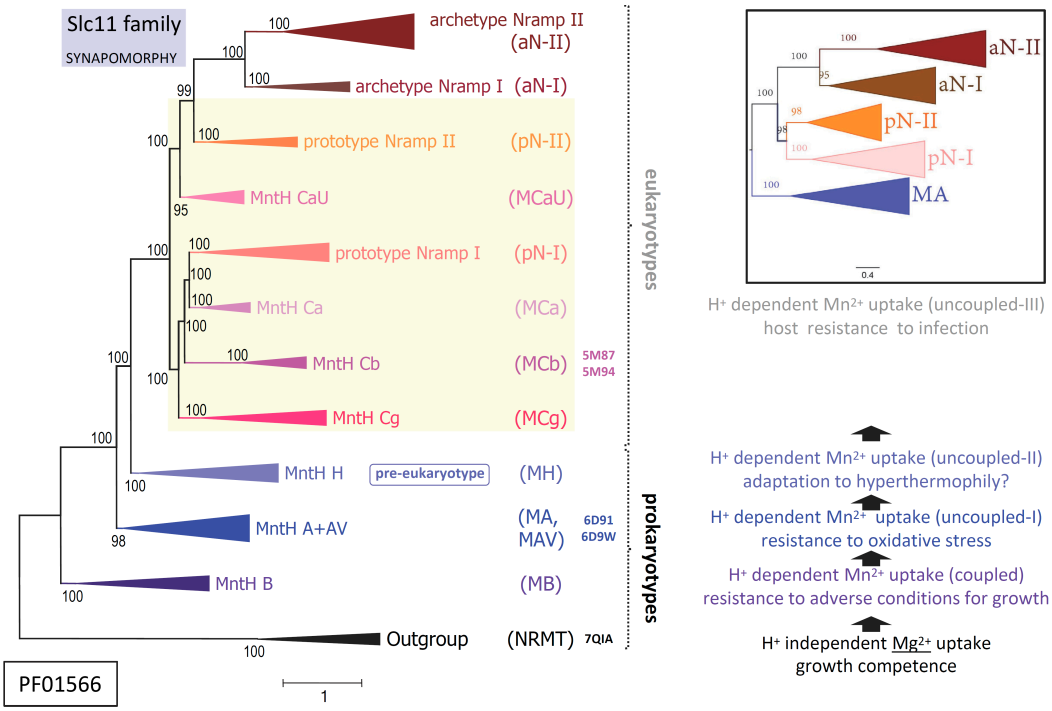


**Figure 1. Functional evolution of Slc11 carriers.** Schematized Slc11 phylogeny (*Left panel* and *Inset)* in the context of stepwise evolution of Slc11 $H^+$-network interacting with the transmembrane proton motive force to drive $Mn^{2+}$ import (*Right panel*). Note monophyly of bacterial clades MntH Ca, Cb, Cg and eukaryotic Nramp pN-I, as well as established relationships for eukaryotic prototype and archetype *Nramp* parologs (pNs and aNs, respectively, *Inset*), adapted from [12]. Slc11 synapomorphy is detailed in Figure S8. The phylogenetic position of solved structures is color-coded. 7QIA, 6D9W and 5M94 represent carriers inwardly open (IO) while 6D91 and 5M94 exemplify carriers open to out (OO). Eukaryogenesis owes at least partly to some Asgard/TACK archaeum intrinsic ability to manage intracellular bacterial symbiont(s) [13]. Based on pre-eukaryotic Nramp synapomorphy, Asgard/TACK MntH H represents an evolutionary intermediate in the transition from bacterial $Mn^{2+}$ permease to eukaryotic antibacterial defense [12]. On the other hand, bacterial MntH Cs inherited Nramp-derived characters distinguishing them from MntH homologs of bacterial origin (e.g., MntH B, MntH A), which perhaps fostered colonization of specific ecological niches.[10].

Yet detailing the broad phylogeny of Slc11 carriers shows stepwise evolution of a transmembrane $H^+$-network that connects residues (polar or charged) within the rather immobile 'hash module' of the carrier (vs the 'rocking bundle' and 'gating parts') [3,12]. Serial synapomorphies, i.e., sets of co-evolutionary rate-shifts exclusively shared among taxa from successive monophyletic clades across Slc11 phylogeny, showed stepwise evolution of Slc11 $H^+$-network, e.g., as i) Slc11 family arose and ii) early bacteria evolved from anaerobiosis to aerobiosis; when eukaryotic cells iii) emerged and iv) complexified while dealing with potential microbial invaders. Molecular data thus imply Slc11 mechanism coupling the use of the proton motive force to $Me^{2+}$ uptake evolved repeatedly, as novel environmental conditions prevailed (Figure 1, right panel).

Against this backdrop added complexity comes from independent episodes of bacterial piracy of *Nramp* genes (encoding Slc11 eukaryotypes pN-I and pN-II) subsequently disseminated in distinct environmental niches [12]. This process suggests selective gain of function and opportunity for innovation in various infectious settings [14]**.** The elemental nature of Slc11 preferred substrates (Mn and Fe) makes them vital resources highly coveted during infection [15]. For different reasons perhaps, as Fe is indissociable from growth of cells able to handle it safely while Mn is primarily required to resist conditions adverse for growth [16,17]. As competitive import of Fe and/or Mn may confer a survival advantage, including during infection, it likely exerted strong selective pressure on Slc11 carrier efficiency.

 doi:10.20944/preprints202308.1317.v1



Molecular phylogeny indicates the precise mechanism coupling the use of the proton motive force with $Me^{2+}$ uptake differs between MntH clades of bacterial origin (e.g., MntH B, MntH A) and those derived from eukaryotic ancestors (MCa, MCb and MCg on one hand, and on the other hand, MCaU, Figure 1). Bacterial *Nramp* descendants (coding for MntH Cs or MCs) could further diversify by adapting to select ecological niches (e.g., gut of pollinating insects for MCb, and plant rhizosphere for MCg). Interestingly, AF2 modeling of MC sequences yielded two sorts of predictions wherein MCb sequence diversity produced an array of plausible conformers while in contrast, models predicted for MCg, MCa and MCaU xenologs appeared rather stereotypical [12].

Arguably, as MCb structures solved previously were used to train AF2 learning models, subsequent modeling may in turn interpret MCb sequence diversity as available space allowing accurate prediction of various conformers, which could indicate MCb carrier intrinsic flexibility. On the other hand, MC sequences from other groups, e.g., MCg, differ from MCb from two standpoints: a unique founding event followed by independent evolutionary trajectories. It thus seems that the complex evolutionary processes at work constrain AF2 modeling space for other MC subgroups, yielding predicted structures that appear relatively rigid. Difference in intrinsic flexibility of MCb and MCg carriers may reflect divergent adaption of $H^+$-dependent $Mn^{2+}$ import dynamics to selective niches. To investigate this possibility AF2/CF modeling of three MCbs and two MCg1s was subjected to a site-directed mutagenesis scheme designed to either induce or prevent conformation switch to seek evidence of sister group-specific structural divergence of possible functional significance.

To demonstrate MCb AF2/CF models represent functional conformers structural ensembles capturing alternate carrier states, e.g., either outward open to bind substrate, inward open for its intracellular delivery or in-between, were collected. Intramolecular communities of networked residues that would typify these ensembles and could be targets for mutagenesis to probe their role in carrier conformation exchange were identified. A mutational strategy aimed at inducing '*in silico conformation switch*' that would mimic the transition observed between native conformer ensembles was established. To test the hypothesis that Slc11 synapomorphy may constitute a 3D network of conformation switch instructive sites, mutation combinations that reproduced ancestral evolutionary rate-shifts were employed. A suitable genetic background, i.e., mutation combination leading to alternate conformer modeling relative to the native template, was used to question the role of several communities of networked residues. Distinct MCb templates were used to compare results and appreciate shared functional properties.

Knowledge gained from studying MCb in silico conformation switch was applied to characterize its sister clade MCg. To establish MCg1 models as functional conformers, conservation of Slc11 synapomorphy role in conformation exchange was tested with distinct templates. It was determined if MCg1 models undergo similar mutation-induced conformation switch. Template sensitivity to mutation combinations inducing alternate conformer modeling was compared between MCg1s and MCbs, and among divergent MCg1s. Structural, phylogenetic and taxonomic evidence of functional significance relating to the divergence between MCg1 and MCb clades, and amongst them, were gathered to support data interpretation. 3D conservation of conformation switch instructive sites was examined across MCg1 and MCb models. Integrating all the data produced suggests a plausible evolutionary scenario wherein 3D conservation of Slc11 synapomorphy embeds the basic mechanism of carrier conformation exchange, which is maintained at substantial cost in fast evolving MC clades through divergent epistasis.

## 2. Results

### *2.1. AF2/CF predict native MCb carrier cycle intermediates*

Slc11 carriers work by cycling between alternative conformations using the proton motive force to direct $Mn^{2+}$ transport toward cell interior [1,18]. During $Mn^{2+}$ import, Slc11 carrier conformation evolves through a continuum of conformers from OO state (e.g., apo, ion-coupled, metal-bound) to IO state (e.g., metal-bound, ion-coupled, apo) with intermediate conformers (ion-coupled and metal-bound) doubly occluded and including the tipping point for directional transport [5,19]. Notably,

Preprints (www.preprints.org) | NOT PEER-REVIEWED | Posted: 18 August 2023 doi:10.20944/preprints202308.1317.v1



AF2/CF predictions for Uniprot MCb sequences produce an array of 3D models that may represent functional intermediates in the transition between OO and IO states [12].

To infer a temporal sequence of possible structural changes accompanying MCb conformation transition, the solved pdb entries 5M87 and 5M94 were set as reference structures representing distal alternate 3D states (OO and IO, respectively). MCb AF2/CF models were selected among those populating the shortest path linking MCb reference structures in AAA Dali comparisons, including one that seemed close to MCb conformation switch point (Figure S1). Per residue root mean square deviation of the Ca chain (RMSD) from either reference structure was calculated for each candidate conformers selected (Figure S2).

To model structural evolution of MCb carrier during OO to IO transition three candidate conformers, representing hypothetical steps close to MCb switch point (either OO, IO or in-between), were altogether superposed with the reference structures (Figure S3). Initial progression through OO state shows deviation of the pseudo-symmetric segments h1b and h6a, which increases till conversion to IO state accompanied by displacement of h9-h10. Movement h6a/h10 may push h1b toward h5 creating a pivot point for h5 tilt. Bending of h8 in 5M94 structure alters the topology of MCb $H^+$-network and could contribute to open the inner gate via h5.

Detailing motion of h1 and h6 (Figure 2), each helix harboring half a $Me^{2+}$ BS in its center - omitted for clarity, shows synchronous downward progressions of h1b and h6a through OO state, apparently mimicking coordination of a bound substrate $Me^{2+}$ ion. The relocations of h1b and h6a terminate simultaneously while h1aC begins moving toward h5, as demonstrated by AF-A0A1P8Q6E3-F1 switch intermediate. This transition completes through IO states with further outward displacement of h1a, perhaps more realistically modeled using aCF while absent from N-terminally truncated 5M94 structure.

To validate MCb model collection as a set of possible conformers, select models were binned into candidate OO, IO and intermediate categories (Figure S1) to compute consensus networks of interacting amino acids (WebPSN). These analyses associated one community of networked residues with each orientation: OO (h1a,h5,h8) and IO (h6a,h10,h11, Figure S4). The visible timing of creation/disruption of these networks in the series of models used indicates that, as expected for membrane carriers, occlusion of the external $Me^{2+}$ binding site is coordinated with opening of the inner gate.

 doi:10.20944/preprints202308.1317.v1



**Figure 2. Predicted motion of h1&h6 during MCb carrier transition from outward open to inward open.** Motion of helical segments deduced from superposed AF2/CF/aCF models for diverse MCb sequences and solved structures of OO (5M87) and IO (5M94) MCb carriers is indicated with color-coded arrows. The AF2/CF models studied are presented in Figure S1. Using aCF to model Q5HQ64 allows visualizing motion of h1a in IO state (which is absent from 5M94 structure).

Another community of networked residues that evolves during progression toward and throughout IO state (limon intermediate and orange to red ensemble) links h1b, h5, h7, h8 (Figure S5). The limon intermediate maintains OO connection between h1b,h7,h5,h8, which is reduced to h1b,h7,h5 once MCb carrier has switched to IO state. This community may help h5 tilt to open the inner gate as h1b appears connecting (via h10) outer gate closure (h6a,h10,h11) to opening the inner gate (h5,h7,h8).

Two additional communities of networked residues evolve i) either during progression toward and throughout IO states: part of Slc11 $H^+$-network (Figure S6), implying it is dynamic as MCb OO to IO transition proceeds, ii) or during the OO to IO conformation switch (Figure S7), suggesting a role direct for h6b. Based on these data it was concluded that, in absence of $Me^{2+}$ substrate [20], AF2/CF interpret MCb diversity and intrinsic dynamics to confidently predict a collection of carrier cycle intermediates.

*2.2. Site-directed mutagenesis demonstrates the functional significance of MCb Q5HQ64 CF modeling*

Given a suite of valid conformers populating intermediate steps during MCb carrier cycle it should be possible to induce in silico conformation exchange using appropriately targeted mutagenesis: i) to identify sites provoking MCb conformation exchange, and ii) to probe the impact of defined MCb communities of networked residues on this mutation-induced conformation switch.

The evolutionary concept of 'Slc11 synapomorphy' (Figure S8) entails a novel character shared by all the members of this family. This set of synapomorphic amino acid residues, products of type ii co-evolutionary rate-shifts, was previously proposed to contribute to co-substrate binding and carrier gating [12]. Several members of Slc11 synapomorphy were found in communities of networked residues that evolve during OO to IO MCb carrier transition: two h6 sites involved in MCb conformation switch (cf Figure S7) and both h10 and h11 sites mobilized for outer gate closure (cf Figure S4, right panel). Also, relaxing Slc11 synapomorphy definition would include h1a V47/- site (cf below, Q5HQ64 V50 in Figure 4E), which was linked to inner gate opening (Figure S4C, left).

These data support that the 3D network of Slc11 synapomorphy may control carrier conformation transition. To examine this possibility, this set of synapomorphic residues, including the $Me^{2+}$ BS, was targeted using select combinations of mutations that mimicked ancestral type ii evolutionary rate-shifts.

To start a model IO conformer (Q5HQ64) was chosen aiming to mimic backward transition toward the OO state. Q5HQ64 was taken since its AF2 model (magenta, Figure S1) was closest to 5M94. CF pdb top model of Q5HQ64, based on local confidence score (predicted local distance difference test, pLDDT), was obtained using AF2 trained model2 (Figure S9A). Although not ideal, because it shows minimal opening of the inner gate, CF pdb model2 per residue RMSD from reference MCb structures 5M87 and 5M94 indicated it remained part the IO ensemble (closer to orange CF pdb model than magenta AF2 model, data not shown #1), and thus suitable to model mutation-induced conformation back switch.

Q5HQ64 h3 mutation A131Y G135N (h3 YN) is key to switching backward to OO conformation since it cooperates with additional mutations in either h1, h6a, h6b, h7 or h11 to trigger broad scale deviation of the per residue Ca RMSD from the native Q5HQ64 IO conformation (Figure S9BD). The profile of this apparent back switch toward OO state is conserved among the resulting mutants and encompasses h1b-h2N, h5-l5/6-h6a, l7/8-h8N, h9C-h10N, h11C. Coordinated targeting of Q5HQ64 h3 (YN) and additional Slc11 synapomorphic sites therefore mobilized the same helical segments that were noted during transition of native MCbs from OO to IO states.

Preprints (www.preprints.org) | NOT PEER-REVIEWED | Posted: 18 August 2023 doi:10.20944/preprints202308.1317.v1



The influence of h1 $Me^{2+}$ BS mutations depends on the conformation induced by the genetic background on which they were tested: absent in wt (data not shown #2), and in the conformation silent h6 VY mutation (Figure S9D), but large and positive in conformation switch conducive background (h3 YN); small and negative in a switch intermediate (VY YN, i.e., h3 YN h6 VY, Figure S10) and virtually absent in more fully switched OO conformation (h3 YN h6 VY A228T, VNT). These data suggest epistatic interactions consistent with a direct role of h1 $Me^{2+}$ BS in Q5HQ64 conformation exchange.

Combining both h1 $Me^{2+}$ BS mutations reversed some of the effects induced by each mutation assayed separately (Figure S11): it abrogated their strong positive interactions with YN, annulated their weak negative interaction with VY-YN and impacted negatively h7 N277T augmented VY-YN background without affecting VY YN A228T induced conformation switch. This indicates that h1 $Me^{2+}$ BS mutations interact with one another, and this interaction depends on Q5HQ64 conformation. Besides, Q5HQ64 back switched conformation (VY YN A228T, VNT) fits between native MCb conformers green and cyan (Figure S11, inset, and Figure S1&2). These analyses support that Slc11 synapomorphy is instrumental to MCb carrier cycling and indicate an intrinsic role of Slc11 $Me^{2+}$ BS in MCb conformation transition.

*2.3. Central role of h3 in MCb Q5HQ64 in silico IO to OO conformation exchange*

Q5HQ64 h3 YN mutation also cooperates with h10 mutation combination S393A L397N S398G (ANG) albeit moderately (Figure S12A), while in VY YN background, ANG produced a rearrangement slightly deviating from the profile of another triple mutant h6 A228T, h7 N277T and h11 N442G (Ttg), in the area of inter-helix contacts between h3 and h10 [6,7]. Also, h10 ANG cooperated with Ttg in YN background but this was not obvious in VY YN background. In addition, h10 ANG negative influence in VY YN background was not corrected by either h6 A228T, h7 N277T, h11 N442G (Figure S12B) or their paired combinations (Figure S12C), which suggests some role for h3 h10 inter-helix contacts.

Moreover, both in YN and VY YN backgrounds, combining h10 ANG with h11 N442G in the absence of h6 A228T reduced per residue RMSD of the resulting model (Figure S12B), implying limited conformation switch compared with h10 ANG only. Both h10 S398 and h11 N442 are constituents of MCb 5M94 IO community c11 [nc18] (Figure S4C, left) and their combined mutation may impair outer gate function. Together these modeling data therefore suggest direct interaction between h3 and h10 that connects MCb outer gate to Q5HQ64 conformation switch.

The YN mutation places Q5HQ64 h3 at the nexus of inter-helix connections involving other Slc11-specific sites whose combined mutation produce conformation back switch from IO to OO state. And since h3 shows limited motion during OO to IO transition (e.g. Figure S2) it ensues that Q5HQ64 h3 mutations A131Y G135N (YN) may interfere with more mobile elements, such as the $Me^{2+}$ BS (h1 D54, N57 and h6a A228) and/or h10 sites, to favor conformation exchange. Introduction of the orphan outgroup substituents YN deviates h3 locally, possibly relieving interactions normally formed in IO state with h1, h6 and h10 and therefore easing backward model transition toward OO state.

The role of h3 in Q5HQ64 conformation switch was questioned by i) testing an alternative alignment of h3 segment and consequently targeting different sites, whose mutagenesis remained conformation silent (Figure S13), and ii) considering the Slc11 outgroup perspective on h3 original alignment to mutate additional sites (Figure 3).

Preprints (www.preprints.org) | NOT PEER-REVIEWED | Posted: 18 August 2023 doi:10.20944/preprints202308.1317.v1



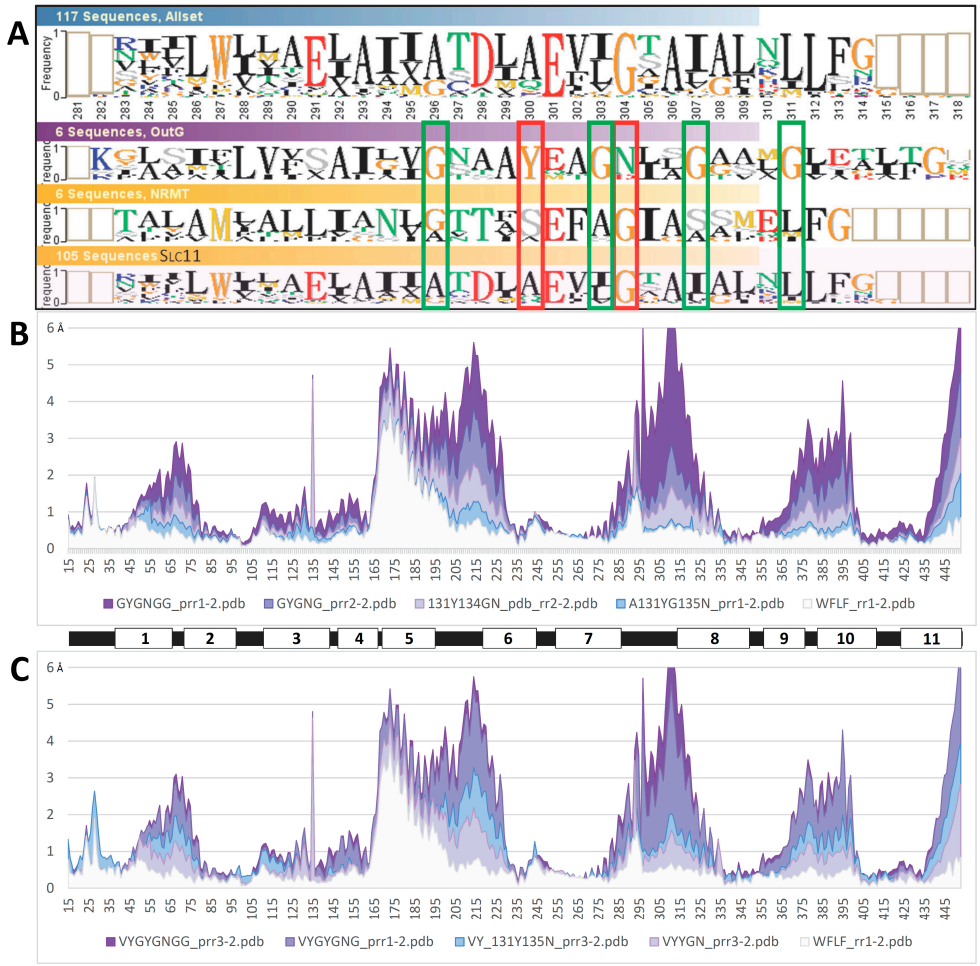


**Figure 3. Impact of h3 topology on Q5HQ64 predicted conformation. A**. Logo display of the multiple sequence alignment with type ii Slc11/outgroup evolutionary rate-shifts indicated in red and outgroup type I evolutionary rate-shifts highlighted in green (i.e., 4 invariant Gs in the orphan OutG only). **B&C**. Impact of outgroup h3 type I evolutionary rate-shifts on Q5HQ64 conformation in YN (Y---N) background (**A**) and VY YN (h3 Y---N and h6 V-Y) background (**B**) shown as per residue RMSD (Ca trace) in Å from (wt Q5HQ64 CF pdb model4 used as proxy to) AF2 initial IO model. Q5HQ64 transmembrane helices are positioned below. WFLF, wt Q5HQ64 CF pdb IO conformer (model2) shows limited opening of l4/5-h5 tilt (inner gate, cf aCF modeling, Figure 2) indicated by substantial local per residue RMSD. Combining h3 mutations induces synchronous locking of the inner gate and broad scale rearrangement switching to OO conformation.

Combined, six h3 mutations (GYGNGG) sufficed to induce maximal broad scale deviation (independent of h6 mutation VY). Compound mutants VY YN 228T and GYGNGG exhibit similar OO profiles that differ at h3 and h10 contact area (Figure S14), suggesting intrinsic flexibility allowing local compensatory rearrangement between these two helices. The data imply that altering h3 topology or curvature can switch Q5HQ64 predicted conformation from IO to OO.

*2.4. MCb 3D models are flexible and share alternate communities of networked residues*

A second round of mutagenesis aimed at testing the role of the communities of networked residues, previously identified using ensembles of native MCb models in different states (OO, intermediate, IO), in the in silico conformation switch modeled between wt Q5HQ64 (IO) and VNT mutant (VY YN 228T, OO).

Preprints (www.preprints.org) | NOT PEER-REVIEWED | Posted: 18 August 2023 doi:10.20944/preprints202308.1317.v1



Site-directed mutagenesis intended to maintain either the inner gate open, using bulkier side chains, or the outer gate closed, providing a possibility for salt bridge, prevented full-scale IO to OO conversion and proper rearrangement of the $Me^{2+}$ BS (Figure 4).

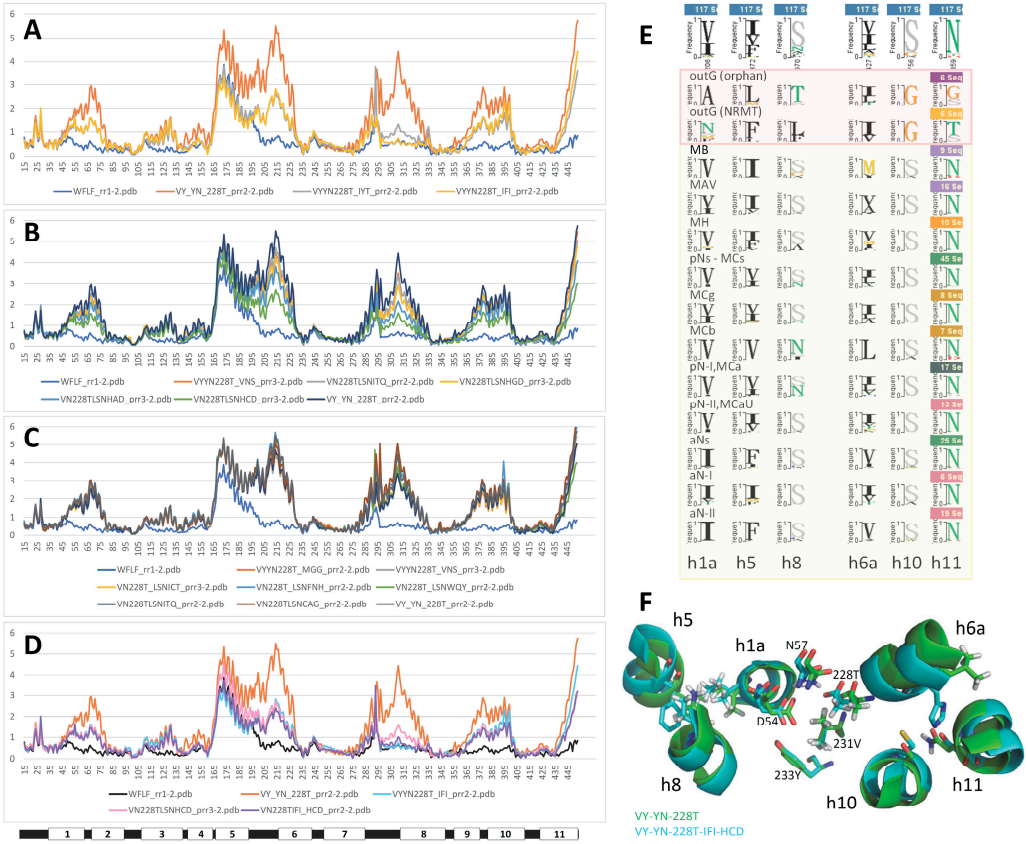


**Figure 4. Targeting MCb alternate communities of networked residues prevents modeling Q5HQ64 conformation back-switch. A-D**. Per residue RMSD of mutant Q5HQ64 (in Å). **A.** Triple mutation targeting 5M87 community 7 (Figure S4) i.e., Q5HQ64 h1a V50, h5 V177, h8 N334. **B, C.** Triple mutation of the 5M94 community 11 [nc18] (Figure S4) i.e., Q5HQ64 h6a L223, h10 S398, h11 N442. **D.** Targeting both 5M87 community 7 (h1a,h5,h8) and 5M94 community 11 [nc18] (h6a,h10,h11) simultaneously. **E.** Natural evolutionary variation of each of the targeted sites. **F.** Impact on the $Me^{2+}$ BS arrangement of the mutations tested.

The data indicate functional significance of the targeted communities of networked residues both in Q5HQ64 conformation exchange induced in silico and more generally, in model MCb carrier cycling.

In contrast, mutagenesis interfering with sites of Slc11 $H^+$ network had little impact (Figure S15), suggesting that either the substitutions assayed were not effective or the sites tested do not contribute to intramolecular rearrangements leading to conformational change. Besides, targeting a community of hydrophobic residues (h1, h5, h7, h8) possibly involved in h5 tilt toward IO state (Figure S5) showed few among the substitution combinations assayed limited the amplitude of per residue RMSD in the areas of h1b and l5/6 & h6a (Figure S16). These combinations represent the consensus sequence of either outgroup (orphan or NRMT) or aN (aN-I or aN-II) clades, which constitute the root and tip of Slc11 family tree, respectively (Figure 1), hence suggesting possible significance.

To verify that properties of Q5HQ64 CF pdb model apply to distinct MCbs, another sequence (WP_002459413, cf Figure S1, 83% identical to Q5HQ64) was shown to respond similarly to the VNT mutation (Figure S17A). In addition, A0A380H8T1 (the closest Uniprot relative of *S. capitis* 5M94, 90% id with Q5HQ64), which produced an IO CF model like Q5HQ64 model, was subjected to identical mutations (Figure S17AD). Some results deviated from the findings of Q5HQ64 study, such that h1 $Me^{2+}$ BS mutations did not cooperate with h3 YN for broad scale rearrangement (Figure S17B), and

Preprints (www.preprints.org) | NOT PEER-REVIEWED | Posted: 18 August 2023 doi:10.20944/preprints202308.1317.v1



VY YN strong sensitivity to h1a D48G mutation (Figure S17C). Yet A0A380H8T1 h3 YN mutation required cooperation with h6 VY mutation to switch wt IO conformation toward OO state and the resulting per residue RMSD was also globally enhanced by combining with h6a A223T. Hence, native IO conformers from distinct MCb respond similarly to compound mutagenesis targeting sites part of Slc11 synapomorphy by switching to OO state.

Modeling of both A0A380H8T1 and WP_002459413 was also highly sensitive to targeting MCb OO community 5M87 c7 (h1a V50, h5 V177, h8 N334), which strongly antagonized VNT (VY-YN-223T) induced conformation switch (Figure S17D,E), having direct effects on h1, h5 and h8 topology (profile resembling that of A0A380H8T1 YN D48G, Figure S17B). Furthermore, mutating sites of 5M94 IO community c11 [nc18] (h6a L223, h10 S398, h11 N442) impacted VNT-induced conformation, as previously observed for Q5HQ64, by decreasing the overall amplitude of the switch (Figure S17D,F). Hence, mutually exclusive communities of networked residues identified among separate pools of native MCb conformers, either OO or IO, control in silico transition from IO to OO state of distinct MCb templates.

Comparing native IO and mutation-induced OO conformers obtained for distinct MCbs (Figure 5) shows pairs of superimposable structures distinguished by coordinate movements of sets of helix segments: i) h1b-h2N [incl. l1/2] and h5-[l5/6]-h6a, and ii) h10N-h9C [incl. l9/10]. Synchronized motion of these segments may complete occlusion of the external $Me^{2+}$ BS while locking the outer gate. MCb IO to OO conformation switch also shows small displacement of h1aC while h6b remains still, as seen in MCb progression from OO to IO state (i.e., between green and orange intermediates, Figure 2). This suggests h1aC early move may initiate opening of the inner gate (unlocking). The 'hash module' helices h3 and h8 in contrast show minimal deviations (except for areas of h3 A-to-Y and G-to-N (YN) mutations, and h8N end), implying they may contribute to carrier conformation switch by interacting with residues from more mobile parts of the structure (e.g., h1 and h10 for h3, and h1a and h5 for h8).

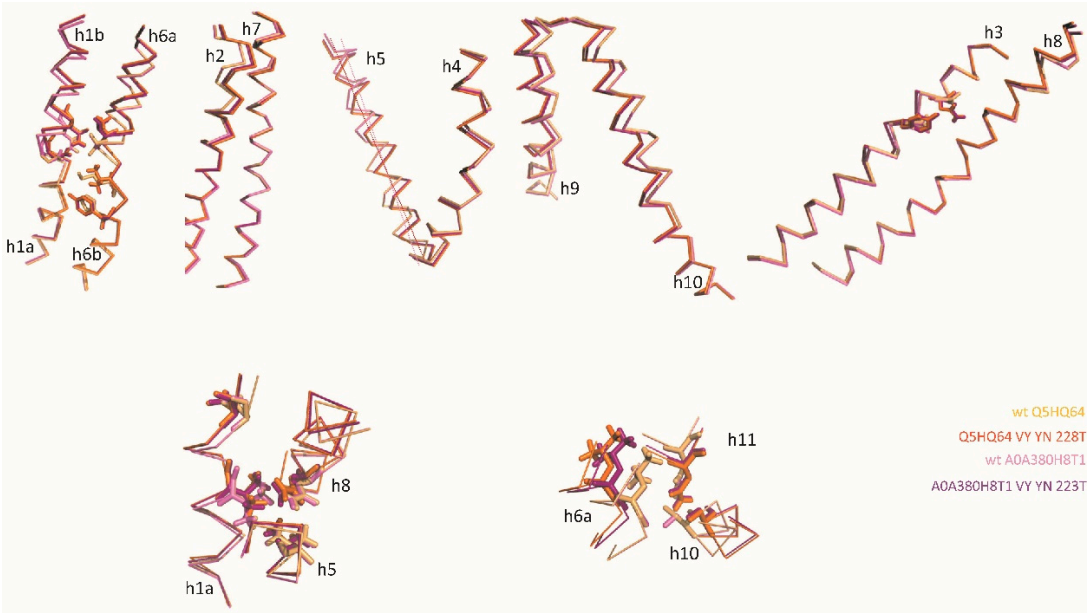


**Figure 5. In silico back-switch of IO to OO conformer is structurally conserved among distinct MCbs.** *Top*. Two pairs of native MCb IO/VNT mutation-induced OO conformers (Q5HQ64 and A0A380H8T1) were superposed, and Ca trace deviations are presented separately for either adjacent or linked helices, as indicated. Sticks show residues forming the substrate binding site (h1 & h6) and the conformation-driving mutation h3 YN. *Bottom*. Details of mutually exclusive communities of networked residues that mediate MCb inner gate opening (left) or that lock outer gate (right).

AF2/CF modeling thus exploits MCb diversity and intrinsic dynamics to confidently predict conformers likely representing discrete steps in carrier cycling. Slc11 synapomorphy comprises MCb

Preprints (www.preprints.org) | NOT PEER-REVIEWED | Posted: 18 August 2023 doi:10.20944/preprints202308.1317.v1



conformation driving sites, including notably prominent contributions of h3, h1/h6 $Me^{2+}$ BS and h10 residues. Specifically, Slc11 synapomorphy is coordinately rearranged during MCb carrier switch (Figure 6A); subsequently, Slc11 synapomorphy deviates minimally albeit significantly (e.g., area of D54, Figure 6B).

Notably, native MCb CF pdb models (Q5HQ64, A0A380H8T1, A0A853V1J2, > 80% id) were superimposable (e.g., Figure 6C) and highly similar to AF-A0A853V1J2 (D54 area, Figure 6B). The 3 MCb VNT CF pdb models are also highly similar, resembling native OO carriers (e.g., AF-Q74JG3, CF pdb-WP_103371048, Figure 6A) as they mimic conformation changes taking place during carrier switch (A, inset) despite local deviation of h3 and h1a (C, inset).

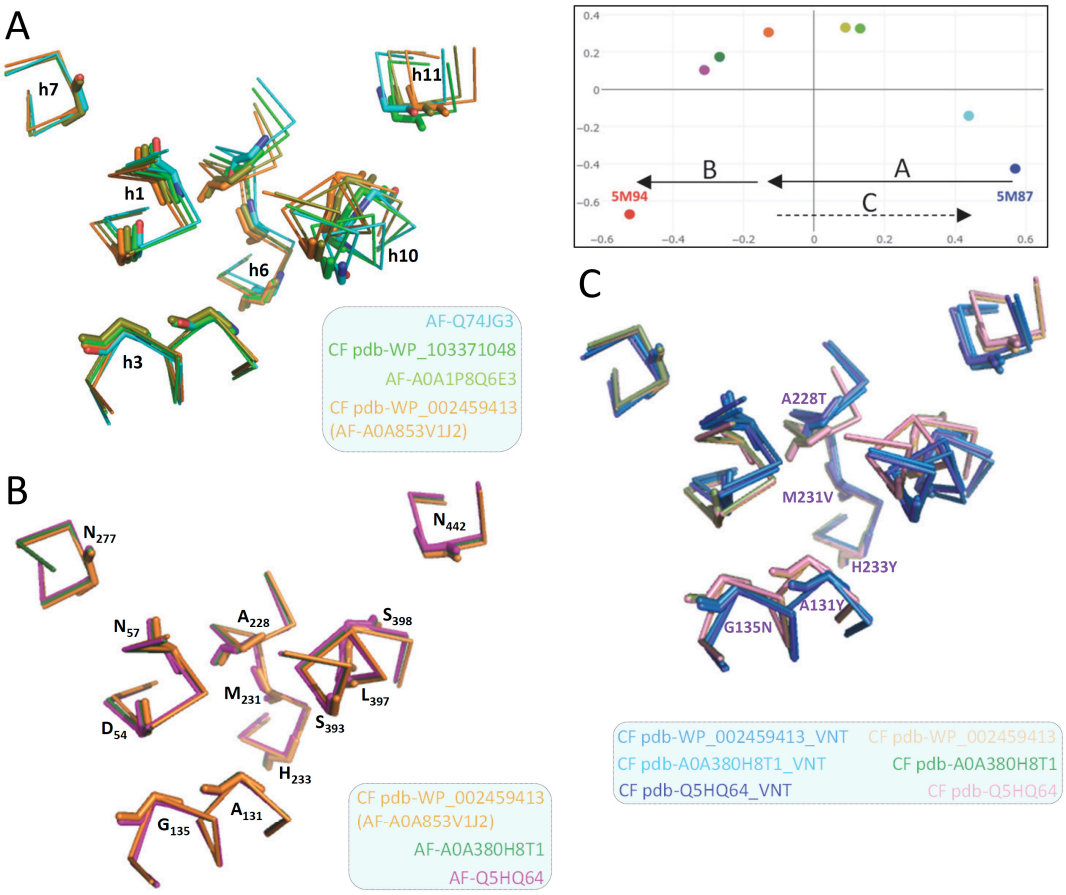


**Figure 6. Slc11 synapomorphy articulates MCb model conformation switch mimicked by the mutation VNT**. Multiple structural model superpositions display the 3D arrangement of Slc11 synapomorphy, indicated by stick representing residues main chains and numbered according to MCb Q5HQ64. For clarity, helix and residue numbers are indicated in separate panels (A & B, respectively) and apply to all 3 panels (A-C). The VNT mutation, i.e., Q5HQ64 h3 A131Y G135N h6 A228T M228V H231Y, is indicated in C. Slc11 synapomorphy 3D arrangement during native MCb model conformation switch (A), subsequently as MCb carriers open inwardly (B), and owing to the VNT mutation (Q5HQ64, A0A380H8T1, WP_002459413, C). *Inset*. Correspondence analysis of MCb models delineating distinct processes: A, carrier OO conformation switch to IO and unlocking of the inner gate, and B, locking of the outer gate and opening of the inner gate. Also, backward switch from IO to OO state that is mimicked by VNT mutation is represented (C, cf Figure S11 *Inset*).

Contrasting with CF pdb predictions of related MCbs (>80% id) that model a single conformer at an early post-switch step (e.g., WP_002459413), their corresponding AF2 models show similar or ensuing steps to open the inner gate, in a sequence-dependent manner (AF-A0A853V1J2<A0A380H8T1<Q5HQ64), with coordinated local deviations of h1a, h5, h7 and h8 (Figure S18A,B) that correspond to two MCb residue communities previously involved with h5 motion (Figure S4, left panel, and Figure S5). Conversely, MCb residue community rather implicated

Preprints (www.preprints.org) | NOT PEER-REVIEWED | Posted: 18 August 2023 doi:10.20944/preprints202308.1317.v1



in h10 motion (Figure S4, right panel) rearrarranges minimally in post-switch steps, suggesting that locking the outer gate is concommitant with complete occlusion of the external $Me^{2+}$ BS (Figure S18C,D,E).

These data suggest MCb carrier OO to IO transition is modeled in two processes: i) a substrate-selective conformation switch that may unlock the inner gate, and ii) post-switch substrate-dependent intracellular release (completing both $Me^{2+}$ BS occlusion and outer gate locking while opening the inner gate). This interpretation is supported by detailing motion of MCb residue communities controlling h5 motion (Figure S18F-I). Their substantial rearrangement during carrier switch could unlock the inner gate (Figure S18F-H) while in subsequent steps, the contributions of h1b and h7 to shift h5 appear selectively reduced (perhaps forming a pivot point) while that of h1a is sustained (Figure S18I).

In sum, Slc11 synapomorphy plays a key role articulating MCb carrier substrate-selective conformation switch and contributes to substrate-dependent intracellular release. As such, it constitutes a set of useful target sites to appreciate structural and functional differences between Slc11 phylogroups in general, and MCb and MCg sister groups in particular.

### *2.5. MCg1 carrier A0A149PND7 undergoes similar in silico conformation switch*

Although MCb and MCg genes derive from a common ancestor [12], none of MCg top models produced by AF2 or obtained through CF pdb modeling grouped with either IO or OO MCb conformer (5M94 and 5M87, respectively; Figure S19). CF nt modeling using AF2 training model 2 gave a candidate IO conformer for A0A149PND7 (MCg1). Using aCF (advanced settings previously used for MCb Q5HQ64) yielded similar IO conformer with slight improvement of the inner gate opening (not shown).

CF nt modeling with default parameters was used to study the impact of site-directed mutations on MCg1 A0A149PND7 predicted conformation because this setting appeared more suitable than advanced CF parameters in prior studies with MCbs.

To examine the role of h3 in MCg1 carrier conformation switch identical mutation combinations were tested in parallel using MCg1 A0A149PND7 and MCb Q5HQ64 templates (Figure S20AB). Unexpectedly, A0A149PND7 h3 A119Y G123N (YN) mutant adopted a fully switched OO conformation, marginally affected by additional h3 mutations, which was further stimulated combined to h6 A216T M219V H221Y mutation (VNT216). The data indicate that similarly to MCb Q5HQ64, A0A149PND7 h3 is key to switching carrier conformation albeit mediating its role in a distinct way. Testing h3 YN mutation with h10 ANG +/- h11 N422G or D (Figure S20C) confirmed this interpretation: cooperation between Q5HQ64 MCb h3 YN and h10 ANG (Figure S12A) was matched by A0A149PND7 h3 YN tolerance for h10 ANG, and in both instances (cf Figure S12B), h11 N422G regulated carrier conformation switch.

To evaluate the contribution of h1 $Me^{2+}$ BS in MCg1 A0A149PND7 conformation switch the mutations D42G and N45T were assayed alone and combined in distinct backgrounds YN, VY and VY YN (Figure S20DEF). Negative impact of D42G combined to h3 YN, and of both D42G and N45T combined to h3 YN h6 VY (VN), were noted. These results support that interaction between h3 YN and h6 VY mutations alters MCg1 A0A149PND7 modeling sensitivity to h1 mutations, as previously observed with MCb Q5HQ64 (cf Figure S11). The data imply Slc11 synapomorphic residues maintained prominent contribution to carrier switch mechanism despite evolutionary divergence of MCb and MCg1.

Targeting the mutually exclusive communities of networked residues identified in ensembles of MCb homologs (Figure S4), and which controlled MCb VNT-driven conformation switch (Figure 4 and Figure S17DE), had mainly local impact and little effect on overall conformation of MCg1 A0A149PND7 VNT (VY YN 226T, Figure S21AF), e.g., deviation of h5 & h4 (A, D), displacement of h6a, h10 & h11 (B, E) or slight outward deviation (tilt) of h5 and minimal impact on h1b, h6a and h10 (C, F). These results suggest differences in carrier intramolecular dynamics consequent to divergent evolution between the sister groups MCb and MCg1.

Preprints (www.preprints.org) | NOT PEER-REVIEWED | Posted: 18 August 2023 doi:10.20944/preprints202308.1317.v1



To explore that aspect further, A0A149PND7 secondary suppressor sites of YN-driven conformation switch were sought by examining YN mutant model. Possible sites of direct contact were located on h1, P43, and h10, L370 and Q374. Mutating P43A alone or combined with N45G had essentially no impact on modeling (Figure 7AB). To obtain substantial effect it was necessary to mimic NRMT sequence in this area, with the 4-residue exchange I41N P43A N45G W46I (NAGI).

Turning to h10, reducing Q374 side chain volume reversed YN induced conformation switch, at least partly, by better accommodating h3 A119Y substitution (Figure 7CD). Combining both h1 and h10 mutations in A0A149PND7 YN background had additive effects resulting in close to wt IO conformation (Figure 7). The data indicate MCg1 A0A149PND7 h3 YN mutation induces conformation switch by alterings inter-helix contacts between h3, h1 and h10.

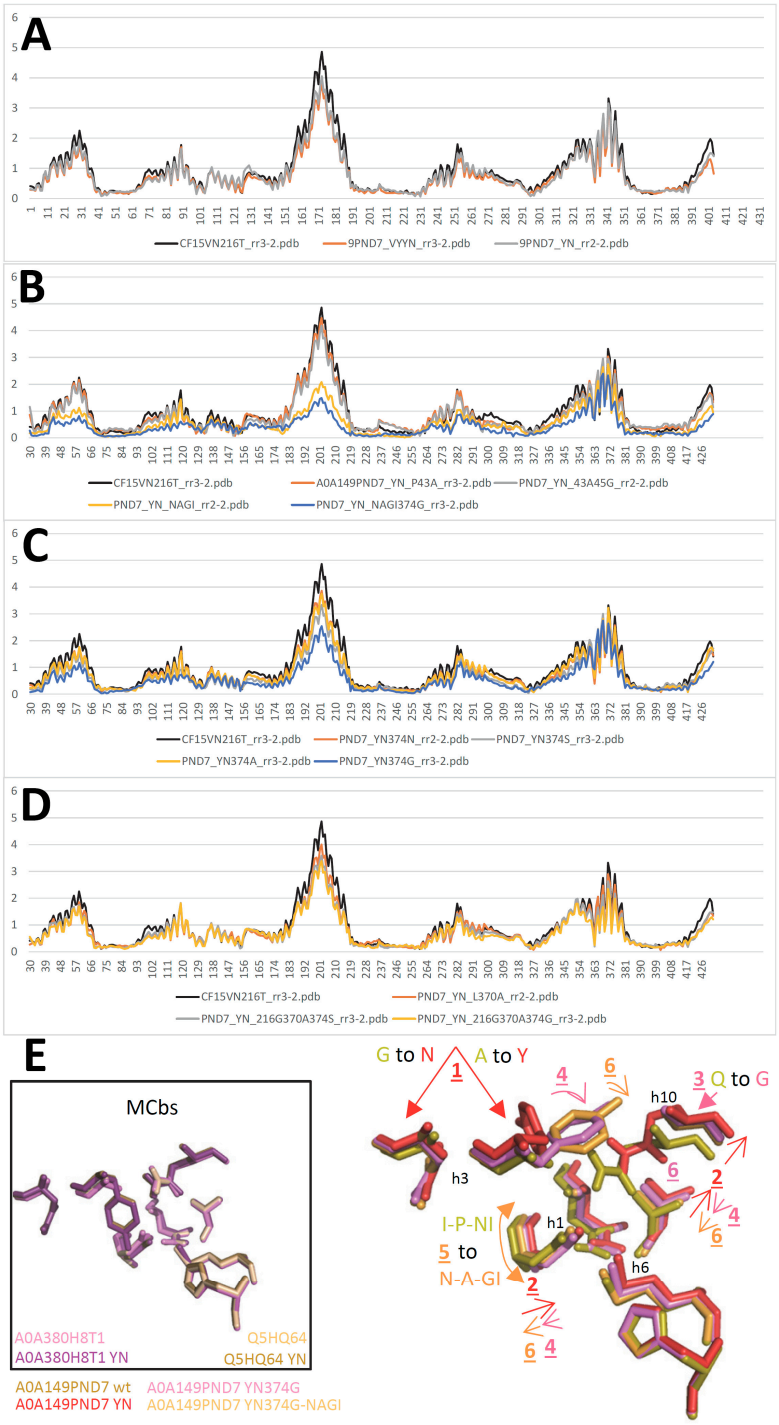


**Figure 7. Site-specific suppression of MCg1 A0A149PND7 h3 YN-driven conformation switch. AD.** Per residue RMSD of A0A149PND7 mutants. **A**. At Slc11-specific sites inducing conformation switch

 doi:10.20944/preprints202308.1317.v1



modeling (h3 YN +/- h6 VY and A216T). **B**. Near h1 $Me^{2+}$ BS and at h10 Q374. **C**. Alternative substitutions at h10 Q374. **D**. Combining h3 YN h10 L370A h6 A216G and h10 Q374S or G. **E**. Superposed structures demonstrate mutagenesis (closed arrowheads) induced deviation (open arrowheads) of select sites in h3, h10, h1 and h6: 1- YN mutation induces 2- Ca deviation of h1, h6 and h10 residues; 3- h10 Q374G mutation allows 4- rearrangement of h3 Y and correction of Ca deviation for h6 and h1 residues; 5- NAGI mutation stimulates 6- further rearrangement of h3 Y and correction of Ca deviation of h6 and h1 residues. *Inset*: Impact of h3 YN mutagenesis on MCb modeling.

Indeed, YN compound mutant 394G, but not NAGI, was rescued by h6 VY mutation to produce YN-like broad scale RMSD (Figure S21G). YN 394G reduced conformation switch was also reverted to YN levels when combined to h6 A216T, h11 N422G or both, but not h7 N264T. And h7 N264T disrupted cooperation between A0A149PND7 mutations YN (h3) A216T (h6) 394G (h10) and N422G (h11) (Figure S21H). Lastly, substituting h11 N422 regulated cooperation between h3 YN h10 Q394G and h10 ANG (Figure S21I).

Introducing h10 Q394G mutation in MCg1 A0A149PND7 YN mutant therefore restored cooperative behavior between mutations targeting synapomorphic sites (h3 YN and h6 VY, h6 A216T, h11 N422G). The similarity of the resulting conformation changes with those previously observed with Q5HQ64 indicates MCb switch mechanism was conserved in A0A149PND7 MCg1. Yet some data obtained studying A0A149PND7 conformation switch, such as the negative influence of h7 N264T mutation and distinct behavior of h3 mutants suggest also a degree of functional divergence.

### *2.6. Conserved switch mechanism in extensively divergent MCg1 from Bordetella-Achromobacter*

To determine whether A0A149PND7 divergent response to targeted mutations is shared among MCgs, another wt model in IO conformation was necessary. CF nt models obtained for MCgs were re-examined in Dali AAA comparisons, including as reference models those from wt MCg1 A0A149PND7 (IO) and its converted form, A0A149PND7 VY YN 226T (OO), together with MCb pair of structures OO (5M87) and IO (5M94) as outgroup instead of the pair of MA structures IO (6D9W) and OO (6D91) previously used.

These reanalyses pointed another MCg1 sequence (s011, D4XFA5), which yielded both IO and OO conformers depending on the training model used (CF nt rr3-5 and CF nt rr1-2, respectively, Figure S22AB). Notably, D4XFA5 VNT induced OO conformer showed minimal sensivity to dual mutation combinations targeting both residue networks involved in MCb carrier gating (i.e., alternate OO community h1a V50, h5 V177, h8 N334 and IO community h6a L223, h10 S398, h11 N442). In contrast, each mutation combination inhibited slightly native D4XFA5 OO profile and showed sigificant impact when assayed together. These data suggest that alternate communities of networked residues involved in MCb gating may play similar roles in MCg1 carriers.

To verify h3 central role in MCg1 conformation switch the mutation series assayed previoulsy with MCg1 A0A149PND7 and MCb Q5HQ64 (cf Figure S19AB) was tested using MCg1 D4XFA5. These data (Figure S22D) show variation on a common theme, wherein the triple mutation GGG triggers defective broasdcale rearrangement that excludes substrate-selective elements, which become mobilized upon combination with YN mutation. The results imply dual roles of D4XFA5 h3 in carrier cycling by providing a conformation switch instructive signal and linking it to reorganization of the $Me^{2+}$ BS.

Modeling D4XFA5 MCg1 mutants resembled more that of MCbs than MCg1 A0A149PND7, showing cooperation of h3 YN and h10 ANG mutations to produce broadscale conformation switch modulated by h11 D421 mutation (Figure S22E, cf S12AB). Functional similarity of D4XFA5 MCg1 and Q5HQ64 MCb also includes cooperation between h3 YN and h6 A216T or h11 D421G, and between h3 YN and h6 VY (VN, Figure S23AB, cf S9CD) though VN profile was insensitive to several mutations (Figure S23B). And similarly to A0A380H8T1 MCb (Figure S17B), D4XFA5 modeling showed lack of interaction between h3 YN and the $Me^{2+}$ BS (Figure S23A).

As with both MCbs and A0A149PND7 MCg1 the impact of $Me^{2+}$ BS mutations depends on D4XFA5 conformation resulting from the genetic background used: both D42G and D42G N45T

Preprints (www.preprints.org) | NOT PEER-REVIEWED | Posted: 18 August 2023 doi:10.20944/preprints202308.1317.v1



mutations abrogate VY YN-induced conformation switch (Figure S23B) but D42G has no effect in VNT background (Figure S23D), implying functional differences between VN and VNT induced conformers. Along similar lines, mutation combinations inducing similar switch (YN A216T and YN D421G, Figure S23A) are differently impacted by adding h1 D42G (Figure S23C).

CF nt modeling of distinct MCg1 carriers therefore recapitulates the conformational changes established previously for MCb carriers, with similar IO to OO conformation switch coordinately mobilizing the same structural elements and induced by similar combinations of synapomorphic mutations (Figure S24). Divergence among the MCg1 carriers studied (41.4 % id) influences the positions of h1a and h6b, as well as h3 and h8, which both seem species-specific rather than conformation-dependent. Yet h1b and h6a movements appear consistent with those previously observed for MCb templates as well as motion of the h9C-h10N ensemble. Limited shift of h1aC below the $Me^{2+}$ BS is also discernable, together with h5 tilt. The data imply similar principles govern both MCb and MCg1 carrier cycling.

It seems also possible that MCg1 divergence altered carrier function. Examination of multiply aligned sequences and superimposed models from MCb and MCg1 sister clades reveals changes in MCg1 $H^+$-network that modify the topology of h4 (Figure S25). MCg1 h4s lack a conserved D residue part of the (pre-) eukaryotic Slc11 $H^+$-network (shared by MntH H and Slc11 eukaryotypes: aNs, pNs & MCs, Figure 1) [12]. CF modeling shows absence of this D moiety is compensated by arranging in its 3D position the adjacent T side chain and consequently deviating the position of h4 (Figure S25, inset). This local rearrangement is also observed with native MCg1 models in IO state (data not shown #3). Arguably, such intromolecular reorganization may preserve the transmembrane $H^+$-network geometry by altering MCg1 carrier shape, and perhaps its activity.

In this context, further evolution in MCg1 clade may bear functional significance. Given that D4XFA5 MCg1 represents one of the most divergent sequences included in Slc11 family set [12], it was surprizing that A0A149PND7 displayed the most distinctive modeling properties. To investigate this further MCg1 phylogeny was detailed.

The extent of divergence of D4XFA5 MCg1 cluster is demonstrated by Maximum Likelihood phylogenetic analysis of NCBI microbial sequences collected using MCg1-selective PHI-Blast search (Figure S26A). The tree presented suggests MCg1 could emerge in Betaproteobacteria (BPB) of the Burkholderiaceae family (310 organisms) [*Burkholderia* > *Paraburkholderia* > *Caballeronia* > *Pandoraea* > *Cupriavidus*] from a common ancestor that was shared with MCg2 (e.g., A0A149PND7). Notably, D4XFA5 MCg1 divergent cluster shows non overlapping taxonomic distribution, restricted to BPB spp. of the Alcaligenaceae family (90 organisms, *Achromobacter* > *Bordetella*) plus another BPB (Rhodocyclaceae), few GPB (Xanthomonadales) and one APB.

Zooming in on D4XFA5 MCg1 cluster reveals *Bordetella* genus could harbour this gene since its origin (Figure S26B), as MCg1 phylogeny supports previously established species relationships in this genus, positioning *B. ansorpii* basal to the divergence of the sister clusters *B. flabilis-B. bronchialis* vs *B. avium-B. hinzii* [21]. In addition, the *B. flabilis-B. bronchialis* cluster includes two *Achromobacter* seqs, while the remaining forms a sister cluster. These data point a likely origin for *A. piechaudii* D4XFA5 encoding gene because homologs from *A. aestuarii*, *A. agilis* and *A. veterisilvae* stand in basal positions, confirming prior studies based on conserved genes [22,23]. Phylogenetic reconstruction of D4XFA5 MCg1 cluster also apparently discriminates clinical from environmental specimens of *Achromobacter* [24–26], implying clock-like behavior that indicates D4XFA5 MCg1 is a functional protein.

Assuming that h4 and internal $H^+$-network reorganization in MCg1 ancestor introduced steric constraints, as evidenced with A0A149PND7 models, their relative absence deduced from D4XFA5 modeling suggests divergent epistasis in this cluster. Arguably, extensive divergence of the D4XFA5 cluster served to restore more canonical carrier dynamics.

Regarding residues that are identical among MCg2 and D4XFA5 MCg1 cluster, but distinct in A0A149PND7 cluster, the results pointed 6 sites spatially connected in two sets of residues from either h1b, l1/2 and h7 or h4 & h8 (Figure S27AC). Considering group-specific residues, 45 sites scattered across transmembrane helices showed high level of spatial colocalization (Figure S27DF),

 doi:10.20944/preprints202308.1317.v1



linking as well h1a and h7, strengthening h4 and h8 connection together with h5; prominent interactions among h3 and h9, l9/10 are very clear, as well as several instances of colocalizing sites involving distinct helices.

Molecular evidence thus supports the view that A0A149PND7 MCg1 cluster may represent an evolutionary intermediate that could be co-opted and further adapted in the emerging *Bordetella-Achromobacter* genus, for instance. Together with modeling and mutagenesis data showing distinct structural dynamics for A0A149PND7 compared to D4XFA5 and MCbs, it seems plausible that divergence of D4XFA5 MCg1 cluster in *Bordetella* aimed at tuning carrier structural dynamics, including MCg1 neo $H^+$-network.

*2.7. Slc11 synapomorphy: a conserved framework articulating carrier cycling in divergent 3D contexts*

Though modeling of VNT (VY YN A228/223/216T) mutants displayed similar backward transition toward OO state for both MCbs and MCg1s (Figure S25), template sensitivity to the mutations tested varied. Notably, steric interference limited A0A149PND7 MCg1 conformational plasticity, both MCg1 templates exhibited limited or negative interaction between h3 YN and h7 264T and displayed altered h4 topology. Global variations in carrier shape was thus examined by correspondence analysis of Dali all-against-all 3D structural comparisons, using pairs of alternate model states (OO & IO) representing the sister groups MCb and MCg1, plus the reference PDB structures from MCb and the distant phylogenetic group MntH A (cf Figure 1; Figure 8).

The results show parallel meta-ensembles (combining both IO and OO states) that clearly delineate MCb models and structures apart from MCg1 models and MA structures (Figure 8A), a result seemingly at odds with Slc11 phylogeny (Figure 1). IO and OO states segregate in both meta-ensembles, and mutagenesis-induced in silico transitions from IO to OO state appear similar for MCb and MCg1 models. These data support common principles governing MCg1 and MCb carrier cycle while divergent 3D features distinguish MCb from MCg1 structures, e.g., MCb sequence divergence and structural variation in l7/8 (data not shown #4) and MCg1 rearranged h4 and $H^+$-network. In other words, the data suggest conservation of carrier mechanism of conformation exchange within divergent 3D contexts.

Focusing on structural divergence between MCb and MCg1, per residue RMSD were calculated between VNT OO mutants, using Q5HQ64 VN228T as reference (Figure 8B). The profile depicting structural variation among MCbs (grey) identifies peaks in the areas of l7/8, l5/6, l1/2, l9/10 as well as h11C, which testify of MCb flexibility. In contrast, MCg1 profiles (in red) appear drastically different, with only few areas showing limited deviations and covering the central part of h1 and h6 ($Me^{2+}$ BS), h3, h5, h7, h10 and h11. Hence MCb and MCg1 VNT-induced OO models display extensive structural differences supporting their grouping in distinct meta-ensembles (Figure 8A).

Preprints (www.preprints.org) | NOT PEER-REVIEWED | Posted: 18 August 2023 doi:10.20944/preprints202308.1317.v1



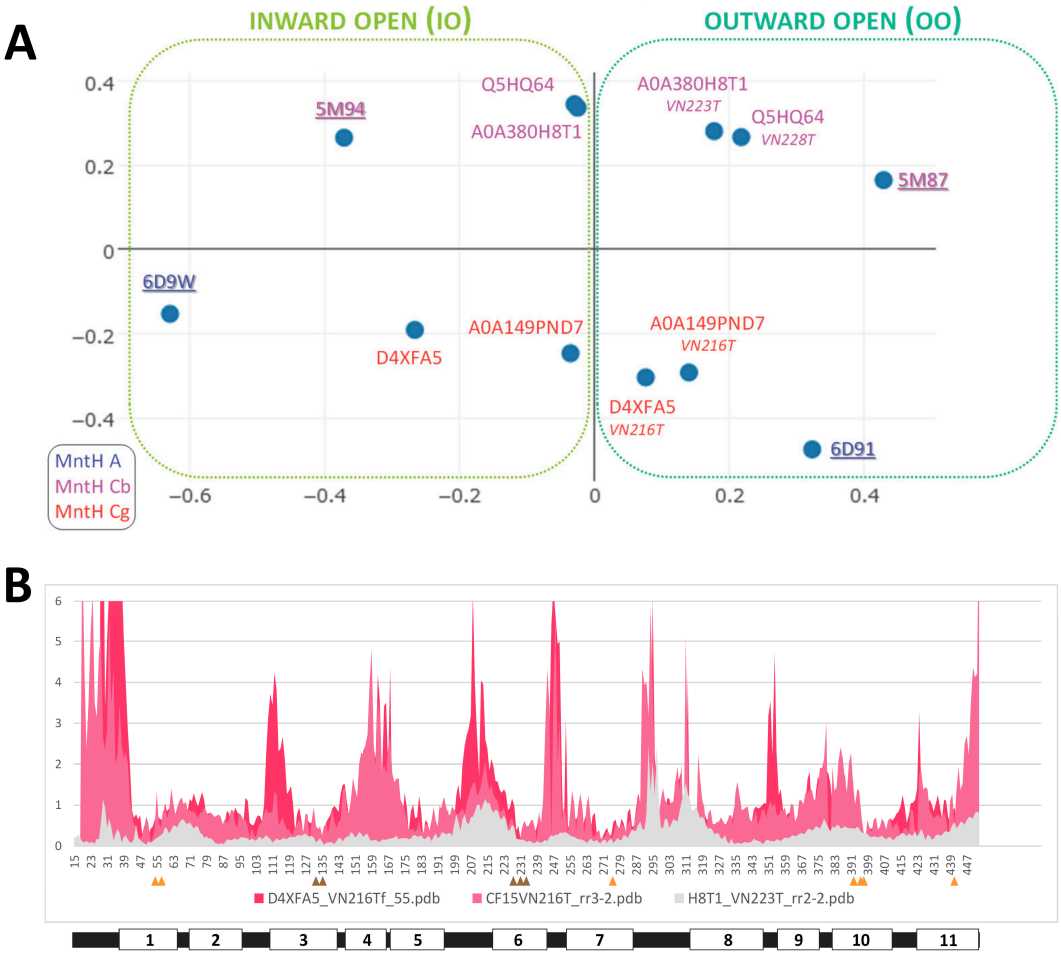


**Figure 8. 3D conservation of Slc11 synapomorphy amid structural divergence of MCb and MCg1 clades. A.** Correspondence analysis of Dali all-against-all structural comparisons using pairs of alternate (OO & IO) states for models representing distinct phylogenetic groups (cf Figure 1): the sister groups MntH Cb and MntH Cg1 (eukaryotic origin), and MntH A (prokaryotic origin). PDB references structures underlined. **B.** Per residue RMSD (Ca) between MCbs (grey) or between MCg1s and Q5HQ64 (red) OO models (VNT mutants). The position of the sites forming Slc11 synapomorphy is indicated by arrowheads (orange, or brown when mutated) and the location of Q5HQ64 transmembrane helices is depicted below.

Yet areas where MCb and MCg1 models deviate least map close to the sites forming Slc11 synapomorphy (respectively, Q5HQ64 h1 D54, N57 and h6 A228, M231, H233; h3 A131, G135; h7 N277; h10 S393, L397, S398; h11 N442), as well as h5 putative pivot point (h5 F188, cf Figure S16, S18GI). These same areas display similarly minimal deviation when native models are compared (data not shown #5). Accordingly, the 3D arrangement of Slc11 synapomorphic sites remained constrained as MCb and MCg diverged and could therefore preserve Slc11 mechanism of conformation exchange within evolving 3D contexts. Indeed, 3D superposition of MCb and MCg1 OO models (VNT mutants) shows little deviation of helix backbone vicinal to Slc11 synapomorphic sites (Figure S25, and also observed with native IO models, not shown), implying that conserved 3D arrangement of these specific areas is instrumental to both MCg and MCb carrier cycling.

Other areas showing 3D morphism between MCb and MCg1, such as h3N and l6/7 (Figure 8B), may contribute as well to maintain the 3D integrity of Slc11 functional network. MCb sequence divergence may promote phylogroup-specific structural variations (e.g. l2/3, h4-l4/5) or even more specific structural determinants (e.g., extensively divergent l7/8 and local deviation of l9/10) that together contribute to the heterogeneity of carrier shapes. On the other hand, 3D neighboring of MCg1 models and solved MA structures (Figure 8A) could reflect structural convergence resulting from MCg1 path of evolutionary divergence (Figure S26).

 doi:10.20944/preprints202308.1317.v1



Based on the data produced through this study a simple interpretation is proposed: Slc11 synapomorphy forms a conserved 3D framework that articulates conformational transition during carrier cycling and whose geometry may be adapted to distinct contexts, because of specific divergence. Indeed, fixation of multiple evolutionary rate-shifts has the potential to create high-order epistasis [27]. Slc11-specific residues would act as functional nodes of a 3D network whose edge dynamics may vary between phylogroups if the respective position of the nodes were coordinately maintained and/or adapted. Under these assumptions, MCb could evolve into highly flexible carriers, providing plastic loops, while in comparison MCg1 adapted to steric constraints (Figure 6) and/or helix distortions (Figure S25).

Together the results obtained argue in favor of functional divergence between the sister groups MCb and MCg because Slc11 core functional network persisted embedded in distinct 3D contexts, which in turn altered intramolecular dynamic properties through functional epitasis depending on local variations in steric hindrance and helix topology. MCg1 D4XFA5 cluster epitomizes functional divergence that correlates with emergence of *Bordetella-Achromobacter* genus, implying potential gain of function.

## 3. Discussion

The biological significance of the present study can be summarized as follows. AF2/CF modeling demonstrates structural divergence of sister groups of bacterial Slc11 carriers of eucaryotic origin, MCb and MCg, which were previously associated with horizontal dissemination amid distinct ecological niches. Coupled to phylogeny-informed site-directed mutagenesis AF2/CF modeling further reveals conservation of a 3D network articulating similar conformation changes within the divergent architectures of MCb and MCg1 carriers. MCg1 site-specific divergence shows steric hindrance altering carrier shape and dynamics and divergent epistasis that correlates with emergence of novel bacterial genera. On the other hand, MCb loop plasticity fosters conformational flexibility. The data suggest different carrier dynamics implying divergent adaptation of $H^+$-dependent $Mn^{2+}$ uptake in distinct environments.

The results presented have methodological implications regarding in silico functional studies of integral membrane proteins using AF2/CF modeling tools combined with phylogeny-aware targeted mutagenesis to better understand sequence/structure/dynamics/function relationships in general, and to appreciate functional correlates of evolutionary divergence between sister clades. The concept of synapomorphy designates a novel character state shared among taxa from a monophyletic clade. Considering a defined protein family as one clade and applying the apomorphy concept to type ii evolutionary rate-shifts (i.e., site-specific replacements of a conserved residue by a novel, also conserved residue) led to short list residues to be targeted to probe carrier conformation switch and permitted direct comparisons across sister clades. Clade-specific paths of divergence were distinguished, wherein a 3D framework articulating carrier conformation switch (Slc11 synapomorphy) is maintained at the cost of local structural deviations impacting carrier shape and dynamics.

MCb plasticity and conformational flexibility likely aid AF2/CF exploiting sequence diversity to model an array of structures representing plausible carrier conformers. Several results established these conformers as functional intermediates: i) binning models of different origins into alternate (OO or IO) or in-between carrier states led to identify communities of networked residues that evolve between these three stages; ii) some of these communities evidenced direct contribution to conformation exchange after site-directed mutagenesis combined with CF pdb modeling using distinct MCb templates; iii) a mutagenesis strategy targeting Slc11 synapomorphic sites produced in silico conformation back switch mobilizing the same helical segments identified among native model conformers; iv) modeling of site-selected MCb mutants showed dynamic responses revealing the central role of h3 linking outer gate closure (h6a,h10,h11) to conformation exchange (h1,h6,h7) and inner gate opening (h1a,h5,h8), including inter-dependent contributions of h1 $Me^{2+}$ BS that hinge on carrier conformational state. These results appeared in line with the basic concepts of carrier-mediated transport [19].

Preprints (www.preprints.org) | NOT PEER-REVIEWED | Posted: 18 August 2023 doi:10.20944/preprints202308.1317.v1



Regarding MCb sister group, MCg, lead results emanated from the divergent subtype MCg1 yielding two native IO conformers used as templates to replicate MCb conformation exchange inducing mutations. MCg1 models underwent similar switch, involving the same helical segments as in MCb models, which signifies conserved switch mechanism, including gating elements, despite divergent evolution. But MCg1 templates' sensitivity to targeted mutagenesis differed, evidencing steric hindrance in one instance apparently compensated by extensive epistatic divergence in another case. MCg1s share a point mutation in h4 eliminating a negative charge part of (eukaryotype) Slc11 $H^+$-network, which appears compensated by distorsion/deviation of h4 to position in its 3D location the adjacent polar residue. Molecular analyses indicate extensive evolutionary coupled divergence that correlates with emergence of the *Bordetella* genus.

An example of conserved functional connection among MCb and MCg1 models, yet subjected to MC group-specific structural constraints is given by h1aC motion during carrier switch. AF2/CF pdb models show strong phylogenetic component, shown with MCbs (Figure S28AD), and limon intermediate conformers (e.g., Figure S1) form a divergent cluster with mutations in h8, among others, including the residue from the networked community (h1a,h5,h8) implicated in inner gate opening (N to S, Figure 4E). Both h8 and h5 sites are rearranged in limon intermediate conformers while most of Slc11 synapomorphy display the expected architecture (except h3 and h7, Figure S28E). Motion of h1aC, shown by MCb limon AF2 intermediates and between native IO and VNT mutation-induced OO CF models of both MCbs and MCg1s, therefore captures an event prior to inner gate opening (unlocking). MCb divergence may impair modeling of h8 interaction with h1aC and result in the prediction of intermediate conformers.

Correspondence analysis of multiple pairwise 3D aligments confirms that MCg1s and MCbs undergo similar mutation-induced conformation exchange; yet extensive structural variation affecting carrier shape underscores divergence between these sister groups. On the one hand, few areas in MC carrier structures show minimal deviation between superposed models of MCb and MCg1 in similar states (IO or OO) and these areas map close to Slc11 synapomorphic sites. Thus, Slc11 synapomorphy represents the 3D preservation of a functional network that articulates metal-selective conformational changes. On the other hand, helical segments that deviate between MCg1 and MCb counterparts represent potential structural constraints that may affect carrier shape and influence the dynamic response to mutagenesis targeting Slc11 3D functional network.

In this regard, it appears significant that extensive epistatic divergence of one MCg1 cluster restores a dynamic response to mutagenesis similar to MCbs vs the other MCg1 cluster. Molecular data suggest MCg1 $H^+$-network amendment/deviation of h4 was a founding event for this subgroup which originated from a common ancestor shared with MCg2 subgroup. In spite of the structural constraints incurred by altering the carrier shape it seems likely, based on taxonomic distribution, that MCg1 isoform represented by A0A149PND7 fulfils a biological role in soil bacteria of the plant rhizosphere. It may thus be surmised that divergence of MCg1 isoform related to D4XFA5 enabled adaptating this role in the emerging *Bordetella* genus.

The functional importance of MCg1 $H^+$-network amendment/deviation of h4 is underscored by a broader evolutionary perspective. During Slc11 evolution, a T moiety appeared in h4 of bacterial MntH A, expanding their internal $H^+$-network. Then, in the common ancestor of archaeal MntH H and Slc11 eukaryotypes (Figure 1) the carrier incorporated among others, an adjacent D residue preceding this h4 T moiety, hereby extending possible interactions between the transmembrane $H^+$-network and the proton motive force driving $Me^{2+}$ import [12]. MC descendants of prototype Nramp possess this h4 D residue, except all MCg1s. The h4 DT pair was most strictly conserved in pN-II, MCg2, aN-II and MCaU. Loss of h4 D is only observed in MCg1 and in aN-I. However, in aN-I *A. thaliana* Nramp1, substitution of D for S apparently preserves both the $H^+$-network and h4 topology (Q9SAH8). These evolutionary patterns add credence to a regulatory role of h4 DT pair and support functional significance of MCg1-specific rearrangement of h4. This suggests MCg1 structure preserves Slc11 $H^+$-network at the expense of the carrier shape and perhaps by altering carrier activity.

Preprints (www.preprints.org) | NOT PEER-REVIEWED | Posted: 18 August 2023 doi:10.20944/preprints202308.1317.v1



By analogy, upholding of Slc11 3D functional core network (Slc11 synapomorphy) in fast evolving clades, such as MCb and MCg1, may impact carrier shape and/or dynamics of transport. Assuming the latter is a driving force for diversification, distinct adaptive paths may lead to clades of carriers whose flexibility and dynamics differ widely. AF2 models for other MC groups (MCa and MCaU) resembled those of MCgs, apparently lacking the conformational flexibility displayed by MCb models [12]. Future studies will be required to determine whether this means additional variety in terms of MC carrier intramolecular dynamics.

From an evolutionary perspective, it is most parsimonious that MCb evolved higher flexibility on their own, in response to selective environmental constraints. Several examples of benefit and/or competitive advantage conferred by genes encoding MCbs have been reported [28,29], and carrier flexibility leading to conformational diversity may contribute to its evolutionary success [20,30]. Besides variations in loop length and sequence, interactions with water molecules may regulate carrier flexibility by forming a network acting to stabilize key residues and/or interaction with the $Me^{2+}$ substrate [31,32]. Also, changes in protein dynamics upon metal binding could have important roles for substrate coordination by the membrane carrier and effective transport [33].

Lastly, this study has biological implications because Slc11 prime substrate, Mn, has shown multifaceted roles in bacterial adaption to stress, including during infection, and in metallo-cross talks that regulate metabolic homeostasis [15,17,34]. In addition, several public health issues relate to the taxonomic distribution of the MntH C sister clades studied here. Estimating non redundant sequence diversity (95% id cutoff) within MC clades previously showed that MCb and MCg were the least represented with about 800 and 400 individual species, respectively, compared to more than one or two thousand counted for MCaU and MCa, respectively. Both MCb and MCg may derive from MCa and display niche-selective, non-overlapping taxonomic distributions [12].

MCb predominates in Mn-centric Lactobacillales, including several pathogens such as *Enterococcus* and *Streptococcus* spp., and it is also prevalent in related bacteria utilizing both Fe and Mn (Bacillales), including *Staphylococci*. *mntH Cb* genes from lactic bacteria used in dairy industry support metabolic activity [29] and competitive exclusion [28]. Participation of *mntH Cb* genes in adaptive responses coping with host nutritional immunity and acid and/or oxidative stress contributes to the virulence of the caries pathogen *S. mutans* [35], group B *Streptococci* [24,36], and the opportunistic pathogens *E. faecalis* [37] and *S. aureus* [38]. To what extent MCb roles owe to intrinsic structural diversity and flexibility awaits further investigation.

MCg is mostly found in iron-centric Proteobacteria from distinct classes (GPB, Pseudomonadales and BPB, Burkholderiales) sharing many properties as environmental soil bacteria frequently found both in the plant rhizosphere and the human flora, including various spp. causing opportunistic infections in immunologically compromised individuals [39,40]. That divergence of MCg1 D4XFA5 clade correlates with the emergence of both *Bordetella* and *Achromobacter* geni (Family, Alcaligenaceae, Order, Burkholderiales) is intriguing [41] and warrants further investigation because they include emerging pathogens associated with resilient nosocomial infections of the lung [25,42,43]. A causal link between MCg1-specific, environmentally constrained adaptation of $H^+$-dependent $Mn^{2+}$ uptake and bacterial pathogenicity, e.g., opportunist lung infection of persons with cystic fibrosis, remains to be addressed.

Deciphering functional evolution of MC clades b and g thus bears potential to gaining important knowledge about Mn availability at distinct interfaces of host cell and microbe interactions. Bacterial species harboring several *mntH Cb* or *mntH Cg* genes are common and may favor diversification through recombination, yielding reservoirs of structural variants. Assuming h4 loss of D mutation altered MCg1 function it seems plausible it was compensated by an array of stabilizing mutations at various sites in the protein, fostering MCg1-specific divergence from its ancestral state [44]. Though epistatic drift through intramolecular interactions may render protein evolution less predictable [45], stressful and/or adverse environments exerting strong selective pressure can channel such process [46]. This seems to be the case with expansive divergence of (D4XFA5) *Bordetella-Achromobacter* MCg1 clade wherein structural divergence suggests shifted constraints that could stabilize MCg1 functional evolution in these emerging bacterial spp.

 doi:10.20944/preprints202308.1317.v1



The present work demonstrated multiple interactions revealed by mutating several sites that form Slc11 synapomorphy, suggesting that collectively, they may produce high-order epistasis and frame evolution of this protein family [27]. Adverse growth conditions, e.g., iron deficiency, severe stress (heat shock, hydrostatic pressure, osmotic stress) that deplete cellular energy (both $Mg^{2+}$ and ATP) or bacteriophage infection [12], may apply sufficient selective pressure to entrench $H^{+}$-dependent $Mn^{2+}$ import function within Slc11 synapomorphy-based 3D framework. In turn, high-order epistasis could accommodate continuous adaptation to function-altering mutations in response to environmental changes, including stepwise elaboration of Slc11 proton-network, loss of h4 D residue in MCg1 proteins, and further evolution in *Bordetella-Achromobacter* genus.

Framing of carrier evolution by high-order epistasis may represent a common property of the LeuT fold: The sheer number of different families it produced showing distinct substrate specificities and using an array chemiosmotic mechanisms to energize transport, yet still sharing properties relating to carrier conformation transition, such as inner gating of h5 and bending of h4, outer gating of h10 and bending of h9, or coordinated motion of h6a and h1b segments [5], together imply the LeuT fold is highly evolvable, meaning intrinsically stable and robust to mutational epistasis [47]. As evolutionary pressure determines long distance evolutionary coupling [48], distinct substrate specificities and/or chemiosmotic mechanisms could shape family-specific high-order epistatic pathways that sustained divergence in the APC superfamily. Maintaining a favourable energy landscape to be traversed during carrier cycling may constrain high-order epistasis [5], and a few residues articulating carrier switch could foster fold evolvability and functional diversity.

To conclude, divergent evolution of MCb and MCg1 affecting carrier shapes and dynamics may be viewed as alternative evolutionary trajectories resulting from different influences [49]. These include i) historical chance for initial founding of each clade and occurrence of function-altering mutations, and ii) high-order epistasis imparted by the 3D conservation of Slc11 synapomorphy, which articulates substrate-selective carrier conformation switch. Prevailing within evolving 3D contexts, Slc11 synapomorphy is thus a reliable phylogenetic marker for function.

## 4. Methods

AF2 3D models for Uniprot MCb sequences were mined for candidate conformers alike MCb reference structures 5M87 (outward open, OO) and 5M94 (inward open, IO) by screening pools of models using EBI all-against-all Dali (AAA) [50], plus a pair of *D. radiodurans* MntH A structures 6D91 (OO) and 6D9W (IO) used as outgroup [51]. Additional models generated through Colabfold (CF) modeling (v1.4 and v1.5.2) [52] using default parameters, including pdb template (CF pdb) or without template (CF nt), and Advanced CF modeling (aCF, parameters: MSA meth Jack hammer, pairwise MSA option 75% coverage, 15%id, max_msa_clusters = 32, max_extra_msa = 64, no use of ptm sampling, num_ensembl 1, max_recycle 1, use is-training, num_sample 1, refine/Amber) [53] were used to explore candidate MC IO models.

A temporal sequence of possible structural changes occurring during OO to IO transition was inferred from graphical representations of per residue Ca root mean square deviation (RMSD) relative to each MCb reference structure (5M87 and 5M94) for each of the conformer selected, established using 2StrucCompare [54]. Structural changes were visualized using Pymol (DeLano, W.L. (2002) The PyMOL Molecular Graphics System. Delano Scientific, San Carlos) display of multiply superposed structures obtained with POSA [55].

Structural communication within MCb molecule was investigated using ensembles of native models representing either OO or IO state. These conformational ensembles were represented as networks of interacting amino acids using webPSN [56]. Consensus networks were computed separately for each ensemble to identify possible structural communication signatures. The outputs were also compared to infer commonalities and/or differences between OO- and IO-states. The functional significance of the communities identified was investigated by site-directed mutagenesis coupled to CF modeling. Two rounds of mutagenesis were performed: first to identify sites involved in MC conformation switch and provoke conformation exchange, and then to probe the impact of candidate communities of interacting residues on this in silico conformation exchange. To this end,

Preprints (www.preprints.org) | NOT PEER-REVIEWED | Posted: 18 August 2023 doi:10.20944/preprints202308.1317.v1



the sequence encoding the closest AF2 model to 5M94 (Q5HQ64) was set as starting material to seek mutation combination(s) that could induce modeling of OO states, i.e., mimicking backward transition from IO to OO conformation.

Site specific evolutionary divergence between MCb and MCg was analyzed using both Diverge 3.0 [57] and Multi-Harmony [58] approaches. Clade-specific consensus sequence at selected sites were displayed using Phylo-mlogo [59]. Molecular genetic evolutionary analysis of MCg1 cluster was initiated using previously characterized sequences [12], plus additional sequences gathered by Psi-Blast searches [60] using either DX4FA5 or A0A149PND7 as queries (cutoff 1e-70). Sequences were aligned using Clustal X [61] and visualized with Phylo-mlogo to derive a MCg1 selective sequence pattern based on the previously established pattern for MCg clade [12]: G[ASP]G[LAVSTIM][LM][VI]AVGY[MIV]DPGNWAT[DEASG]x(30,100)[IVL]A[CT][DA][LV]AE[VIL][IVLA]Gx(5,30)[GAVCSL][TAS][LFYIVC][AVGILST][MLVI]x(50,125)[IVM][LVI]GAT[LVI]MPHN[LI][YF]L[HQ][SGA]x(5,40)[FMLT][LVATIC][VILA]N[SAGL][ASG]x(2,50)[ACS]G[QLM][SN][SA][TA][VLI]T[GAS]. This MCg1-selective pattern used with either DX4FA5 or A0A149PND7 query returned identical PHI-BLAST outputs, which were used as proxy for MCg1 taxonomic distribution. MCg1 seqs were grouped based on pairwise identity before further selection for phylogenetic analysis as previously described [12,62–64].

To test the evolutionary scenario that MCg $H^+$-network was altered in MCg1 and that further divergence of D4XFA5 cluster tuned MCg1 carrier dynamics, sites which underwent successive changes among MCg clusters were sought to determine whether they would co-localize spatially and demonstrate possible evolutionary coupling. Specifically, divergent subsitutions of MCg2 residues that correlated first with MCg1 emergence and then with divergence of D4XFA5 cluster. Two test cases were examined: i) sites showing identical residues in MCg2 and D4XFA5 clusters but distinct in A0A149PND7 cluster, and ii) sites showing cluster-specific residue subsitutions.

To increase chances of detecting signals 3 sets of 11 representative sequences were assembled: one comprising diverse MCg2 seqs [12], another being MCg1 'crown' cluster (A0A149PND7), and the latter *Achromobacter-Bordetella* D4XFA5 MCg1 cluster (Figure S27A). Notions supporting this choice were i) MCg2 diversity may capture the evolutionary processes operating in this clade as a whole, while ii) narrow sampling of A0A149PND7 and D4XFA5 MCg1 clusters may indicate discrete divergent steps. The 33 sequences were aligned and subjected as 3 groups of 11 sequences to Multi-Harmony analysis. Sites ranking as the most significant with both Mutli-Relief and Multi-Harmony approaches (exhibiting both z-weight>6 and z-score<-10, respectively) were mapped on MCg1 models.

**Supplementary Materials:** The following supporting information can be downloaded at the website of this paper posted on Preprints.org, Figure S1. AF2/CF modeling of various MCb predicts a series of possible conformers in carrier cycle, Figure S2. Per residue RMSD of AF2/CF MCb models relative to both MCb reference structures for each candidate conformer selected, Figure S3. Progression in predicted intramolecular rearrangements during MCb OO to IO transition, Figure S4. Alternate communities of networked residues distinguish MCb OO from IO states, Figure S5. Community of hydrophobic residues evolving during MCb transition from OO to IO states, Figure S6. MCb $H^+$-network evolves during OO to IO conformation switch, Figure S7. Alternate h6b connections during MCb OO to IO conformation switch, Figure S8. Synapomorphy distinguishing the Slc11 family from phylogenetic outgroups (all part of PFAM01566), Figure S9. Choice of AF2 trained model2 output (of CF modeling with pdb template) for MCb Q5HQ64 mutagenesis study, Figure S10. Conformational response to h1 $Me^{2+}$ BS point mutations depends on Q5HQ64 genetic background, Figure S11. Mutations of Q5HQ64 h1a and h1b $Me^{2+}$ BS have interdependent effects, Figure S12. Evidence for direct interaction between MCb Q5HQ64 h3 and h10, Figure S13. Testing h3 multiple sequence alignment and deduced selection of targeted sites for mutagenesis, Figure S14. Accommodation of h3 YN mutation in Q5HQ64 compound mutants VY YN 228T and GYGNGG ANG N442D, Figure S15. Effect of mutations targeting Slc11 $H^+$-network on CF pdb modeling of Q5HQ64 VNT (VY YN A228T) mutant, Figure S16. Interaction of h1b, h5, h7 and h8 may regulate coordinated motion of h1b-l1/2 and h6a in Q5HQ64 VY YN A228T, Figure S17. In silico mutagenesis of MCb gating communities prevents VNT-induced switch of CF pdb MCb models, Figure S18. MCb transition from OO to IO comprises two successive processes distinguished by AF2 vs CF pdb modeling, Figure S19. Structural variation among MCg models obtained with either CF with pdb template (CF pdb) or CF with no template (CF nt), Figure S20. h3 YN mutation switching MCg1 A0A149PND7 IO conformation to OO state is modulated by other synapormorphic sites (h1, h6, h10 and h11), Figure S21. Structural divergence of

MCg1 A0A149PND7 from MCbs, Figure S22. CFnt models candidate alternate conformers of MCg1 D4XFA5, Figure S23. Influence of Slc11 synapomorphic site mutagenesis on MCg1 D4XFA5 conformation switch, Figure S24. Similar switch of IO to OO conformers among divergent MCg1s, Figure S25. 3D arrangement of Slc11 synapomorphy is conserved among MCbs and MCg1s, Figure S26. Phylogeny of MCg1, Figure S27. Divergence of the clusters represented by A0A149PND7 (MCg1 crown) and D4XFA5 (MCg1 ABbBf/Bordetella-Achromobacter) shows 3D colocalization of evolutionary coupled mutations.

**Author Contributions:** M.C. is sole author.

**Funding:** This research received no external funding

**Data Availability Statement:** All the models used in this study are deposited in the FigAid repository.

**Acknowledgments:** CF/AF2 online services and support from S. Ovchinnikov and M. Mirdita, the WebPSN server (A.N. Felline), the 2Struccompare server (E. Drew), the Uniprot (EMBL's European Bioinformatics Institute, Cambridge, UK) and National Library of Medicine online facilities (NCBI, Washington DC), including BLAST servers, sequence and model structure repositories, taxonomy browser, and the Dali server (L. Holm) are gratefully acknowledged as well as each contributing Genome Sequencing Project, Godzik's webserver POSA, the IQ-Tree servers, the Multi-Harmony web server, the computational genomics and evolution server (Diverge), the Max Planck Institute Bioinformatics Toolkit Server (Tübingen, Germany), and the Wellcome Trust supported PubMLST.org integrated microbial database.

**Conflicts of Interest:** The author declares no conflict of interest.

## Appendix A

Contains additional data included solely for the purpose of peer review (data not shown #1-5).

## References

1. Bozzi, A. T.; Gaudet, R., Molecular Mechanism of Nramp-Family Transition Metal Transport. *J Mol Biol* **2021,** 433, (16), 166991.
2. Shawki, A.; Knight, P. B.; Maliken, B. D.; Niespodzany, E. J.; Mackenzie, B., H(+)-coupled divalent metal-ion transporter-1: functional properties, physiological roles and therapeutics. *Curr Top Membr* **2012,** 70, 169-214.
3. Forrest, L. R.; Rudnick, G., The rocking bundle: a mechanism for ion-coupled solute flux by symmetrical transporters. *Physiology (Bethesda)* **2009,** 24, 377-86.
4. Yamashita, A.; Singh, S. K.; Kawate, T.; Jin, Y.; Gouaux, E., Crystal structure of a bacterial homologue of Na+/Cl--dependent neurotransmitter transporters. *Nature* **2005,** 437, (7056), 215-23.
5. Del Alamo, D.; Meiler, J.; McHaourab, H. S., Principles of Alternating Access in LeuT-fold Transporters: Commonalities and Divergences. *J Mol Biol* **2022,** 434, (19), 167746.
6. Ehrnstorfer, I. A.; Geertsma, E. R.; Pardon, E.; Steyaert, J.; Dutzler, R., Crystal structure of a SLC11 (NRAMP) transporter reveals the basis for transition-metal ion transport. *Nat Struct Mol Biol* **2014,** 21, (11), 990-6.
7. Ehrnstorfer, I. A.; Manatschal, C.; Arnold, F. M.; Laederach, J.; Dutzler, R., Structural and mechanistic basis of proton-coupled metal ion transport in the SLC11/NRAMP family. *Nat Commun* **2017,** 8, 14033.
8. Ramanadane, K.; Straub, M. S.; Dutzler, R.; Manatschal, C., Structural and functional properties of a magnesium transporter of the SLC11/NRAMP family. *Elife* **2022,** 11.
9. Cellier, M. F., Nramp: from sequence to structure and mechanism of divalent metal import. *Curr Top Membr* **2012,** 69, 249-93.
10. Romei, M.; Sapriel, G.; Imbert, P.; Jamay, T.; Chomilier, J.; Lecointre, G.; Carpentier, M., Protein folds as synapomorphies of the tree of life. *Evolution* **2022,** 76, (8), 1706-1719.
11. Gupta, R. S., Protein signatures (molecular synapomorphies) that are distinctive characteristics of the major cyanobacterial clades. *Int J Syst Evol Microbiol* **2009,** 59, (Pt 10), 2510-26.
12. Cellier, M. F. M., Nramp: Deprive and conquer? *Front Cell Dev Biol* **2022,** 10, 988866.
13. Raval, P. K.; Garg, S. G.; Gould, S. B., Endosymbiotic selective pressure at the origin of eukaryotic cell biology. *Elife* **2022,** 11.
14. Cellier, M. F.; Courville, P.; Campion, C., Nramp1 phagocyte intracellular metal withdrawal defense. *Microbes Infect* **2007,** 9, (14-15), 1662-70.
15. Antelo, G. T.; Vila, A. J.; Giedroc, D. P.; Capdevila, D. A., Molecular Evolution of Transition Metal Bioavailability at the Host-Pathogen Interface. *Trends Microbiol* **2021,** 29, (5), 441-457.
16. Morey, J. R.; McDevitt, C. A.; Kehl-Fie, T. E., Host-imposed manganese starvation of invading pathogens: two routes to the same destination. *Biometals* **2015,** 28, (3), 509-19.
17. Čapek, J.; Večerek, B., Why is manganese so valuable to bacterial pathogens? *Front Cell Infect Microbiol* **2023,** 13, 943390.

18. Nelson, N.; Sacher, A.; Nelson, H., The significance of molecular slips in transport systems. *Nat Rev Mol Cell Biol* **2002,** 3, (11), 876-81.
19. Beckstein, O.; Naughton, F., General principles of secondary active transporter function. *Biophys Rev (Melville)* **2022,** 3, (1), 011307.
20. Banerjee, A.; Saha, S.; Tvedt, N. C.; Yang, L. W.; Bahar, I., Mutually beneficial confluence of structure-based modeling of protein dynamics and machine learning methods. *Curr Opin Struct Biol* **2023,** 78, 102517.
21. Bridel, S.; Bouchez, V.; Brancotte, B.; Hauck, S.; Armatys, N.; Landier, A.; Mühle, E.; Guillot, S.; Toubiana, J.; Maiden, M. C. J.; Jolley, K. A.; Brisse, S., A comprehensive resource for Bordetella genomic epidemiology and biodiversity studies. *Nat Commun* **2022,** 13, (1), 3807.
22. Dumolin, C.; Peeters, C.; Ehsani, E.; Tahon, G.; De Canck, E.; Cnockaert, M.; Boon, N.; Vandamme, P., Achromobacter veterisilvae sp. nov., from a mixed hydrogen-oxidizing bacteria enrichment reactor for microbial protein production. *Int J Syst Evol Microbiol* **2020,** 70, (1), 530-536.
23. Kim, S. C.; Chung, S. O.; Lee, H. J., Achromobacter aestuarii sp. nov., Isolated from an Estuary. *Curr Microbiol* **2021,** 78, (1), 411-416.
24. Aggarwal, S.; Kumaraswami, M., Managing Manganese: The Role of Manganese Homeostasis in Streptococcal Pathogenesis. *Front Cell Dev Biol* **2022,** 10, 921920.
25. Gabrielaite, M.; Nielsen, F. C.; Johansen, H. K.; Marvig, R. L., Achromobacter spp. genetic adaptation in cystic fibrosis. *Microb Genom* **2021,** 7, (7).
26. Jolley, K. A.; Bray, J. E.; Maiden, M. C. J., Open-access bacterial population genomics: BIGSdb software, the PubMLST.org website and their applications. *Wellcome Open Res* **2018,** 3, 124.
27. Miton, C. M.; Buda, K.; Tokuriki, N., Epistasis and intramolecular networks in protein evolution. *Curr Opin Struct Biol* **2021,** 69, 160-168.
28. Siedler, S.; Rau, M. H.; Bidstrup, S.; Vento, J. M.; Aunsbjerg, S. D.; Bosma, E. F.; McNair, L. M.; Beisel, C. L.; Neves, A. R., Competitive Exclusion Is a Major Bioprotective Mechanism of Lactobacilli against Fungal Spoilage in Fermented Milk Products. *Appl Environ Microbiol* **2020,** 86, (7).
29. van Mastrigt, O.; Di Stefano, E.; Hartono, S.; Abee, T.; Smid, E. J., Large plasmidome of dairy Lactococcus lactis subsp. lactis biovar diacetylactis FM03P encodes technological functions and appears highly unstable. *BMC Genomics* **2018,** 19, (1), 620.
30. Juritz, E.; Palopoli, N.; Fornasari, M. S.; Fernandez-Alberti, S.; Parisi, G., Protein conformational diversity modulates sequence divergence. *Mol Biol Evol* **2013,** 30, (1), 79-87.
31. Ilgü, H.; Jeckelmann, J. M.; Kalbermatter, D.; Ucurum, Z.; Lemmin, T.; Fotiadis, D., High-resolution structure of the amino acid transporter AdiC reveals insights into the role of water molecules and networks in oligomerization and substrate binding. *BMC Biol* **2021,** 19, (1), 179.
32. Ray, S.; Berry, S. P.; Wilson, E. A.; Zhang, C. H.; Shekhar, M.; Singharoy, A.; Gaudet, R., High-resolution structures with bound Mn(2+) and Cd(2+) map the metal import pathway in an Nramp transporter. *Elife* **2023,** 12.
33. Serrano, F. A.; Yukl, E. T., Contributions of Conformational Flexibility to High-Affinity Zinc Binding in the Solute Binding Protein AztC. *ACS Omega* **2022,** 7, (4), 3768-3774.
34. Martin, J. E.; Waters, L. S., Regulation of Bacterial Manganese Homeostasis and Usage During Stress Responses and Pathogenesis. *Front Mol Biosci* **2022,** 9, 945724.
35. Kajfasz, J. K.; Katrak, C.; Ganguly, T.; Vargas, J.; Wright, L.; Peters, Z. T.; Spatafora, G. A.; Abranches, J.; Lemos, J. A., Manganese Uptake, Mediated by SloABC and MntH, Is Essential for the Fitness of Streptococcus mutans. *mSphere* **2020,** 5, (1).
36. Shabayek, S.; Bauer, R.; Mauerer, S.; Mizaikoff, B.; Spellerberg, B., A streptococcal NRAMP homologue is crucial for the survival of Streptococcus agalactiae under low pH conditions. *Mol Microbiol* **2016,** 100, (4), 589-606.
37. Colomer-Winter, C.; Flores-Mireles, A. L.; Baker, S. P.; Frank, K. L.; Lynch, A. J. L.; Hultgren, S. J.; Kitten, T.; Lemos, J. A., Manganese acquisition is essential for virulence of Enterococcus faecalis. *PLoS Pathog* **2018,** 14, (9), e1007102.
38. Kehl-Fie, T. E.; Zhang, Y.; Moore, J. L.; Farrand, A. J.; Hood, M. I.; Rathi, S.; Chazin, W. J.; Caprioli, R. M.; Skaar, E. P., MntABC and MntH contribute to systemic Staphylococcus aureus infection by competing with calprotectin for nutrient manganese. *Infect Immun* **2013,** 81, (9), 3395-405.
39. Currie, B. J., Melioidosis and Burkholderia pseudomallei : progress in epidemiology, diagnosis, treatment and vaccination. *Curr Opin Infect Dis* **2022,** 35, (6), 517-523.
40. Tavares, M.; Kozak, M.; Balola, A.; Sá-Correia, I., Burkholderia cepacia Complex Bacteria: a Feared Contamination Risk in Water-Based Pharmaceutical Products. *Clin Microbiol Rev* **2020,** 33, (3).
41. Li, X.; Hu, Y.; Gong, J.; Zhang, L.; Wang, G., Comparative genome characterization of Achromobacter members reveals potential genetic determinants facilitating the adaptation to a pathogenic lifestyle. *Appl Microbiol Biotechnol* **2013,** 97, (14), 6413-25.
42. Bonis, B. M.; Hunter, R. C., JMM Profile: Achromobacter xylosoxidans: the cloak-and-dagger opportunist. *J Med Microbiol* **2022,** 71, (5).

43. Menetrey, Q.; Aujoulat, F.; Chiron, R.; Jumas-Bilak, E.; Marchandin, H.; Dupont, C., A new perspective on opportunistic pathogens of the genus Bordetella in cystic fibrosis. *J Cyst Fibros* **2022,** 21, (2), 344-347.
44. Storz, J. F., Compensatory mutations and epistasis for protein function. *Curr Opin Struct Biol* **2018,** 50, 18-25.
45. Park, Y.; Metzger, B. P. H.; Thornton, J. W., Epistatic drift causes gradual decay of predictability in protein evolution. *Science* **2022,** 376, (6595), 823-830.
46. Ghenu, A. H.; Amado, A.; Gordo, I.; Bank, C., Epistasis decreases with increasing antibiotic pressure but not temperature. *Philos Trans R Soc Lond B Biol Sci* **2023,** 378, (1877), 20220058.
47. Buda, K.; Miton, C. M.; Fan, X. C.; Tokuriki, N., Molecular determinants of protein evolvability. *Trends Biochem Sci* **2023**.
48. Echave, J., Evolutionary coupling range varies widely among enzymes depending on selection pressure. *Biophys J* **2021,** 120, (20), 4320-4324.
49. Starr, T. N.; Picton, L. K.; Thornton, J. W., Alternative evolutionary histories in the sequence space of an ancient protein. *Nature* **2017,** 549, (7672), 409-413.
50. Holm, L.; Laiho, A.; Törönen, P.; Salgado, M., DALI shines a light on remote homologs: One hundred discoveries. *Protein Sci* **2023,** 32, (1), e4519.
51. Bozzi, A. T.; Zimanyi, C. M.; Nicoludis, J. M.; Lee, B. K.; Zhang, C. H.; Gaudet, R., Structures in multiple conformations reveal distinct transition metal and proton pathways in an Nramp transporter. *Elife* **2019,** 8.
52. Mirdita, M.; Schütze, K.; Moriwaki, Y.; Heo, L.; Ovchinnikov, S.; Steinegger, M., ColabFold: making protein folding accessible to all. *Nat Methods* **2022,** 19, (6), 679-682.
53. Pasquadibisceglie, A.; Leccese, A.; Polticelli, F., A computational study of the structure and function of human Zrt and Irt-like proteins metal transporters: An elevator-type transport mechanism predicted by AlphaFold2. *Front Chem* **2022,** 10, 1004815.
54. Drew, E. D.; Janes, R. W., 2StrucCompare: a webserver for visualizing small but noteworthy differences between protein tertiary structures through interrogation of the secondary structure content. *Nucleic Acids Res* **2019,** 47, (W1), W477-w481.
55. Li, Z.; Natarajan, P.; Ye, Y.; Hrabe, T.; Godzik, A., POSA: a user-driven, interactive multiple protein structure alignment server. *Nucleic Acids Res* **2014,** 42, (Web Server issue), W240-5.
56. Felline, A.; Seeber, M.; Fanelli, F., PSNtools for standalone and web-based structure network analyses of conformational ensembles. *Comput Struct Biotechnol J* **2022,** 20, 640-649.
57. Gu, X.; Zou, Y.; Su, Z.; Huang, W.; Zhou, Z.; Arendsee, Z.; Zeng, Y., An update of DIVERGE software for functional divergence analysis of protein family. *Mol Biol Evol* **2013,** 30, (7), 1713-9.
58. Brandt, B. W.; Feenstra, K. A.; Heringa, J., Multi-Harmony: detecting functional specificity from sequence alignment. *Nucleic Acids Res* **2010,** 38, (Web Server issue), W35-40.
59. Shih, A. C.; Lee, D. T.; Peng, C. L.; Wu, Y. W., Phylo-mLogo: an interactive and hierarchical multiple-logo visualization tool for alignment of many sequences. *BMC Bioinformatics* **2007,** 8, 63.
60. Zhang, Z.; Schäffer, A. A.; Miller, W.; Madden, T. L.; Lipman, D. J.; Koonin, E. V.; Altschul, S. F., Protein sequence similarity searches using patterns as seeds. *Nucleic Acids Res* **1998,** 26, (17), 3986-90.
61. Larkin, M. A.; Blackshields, G.; Brown, N. P.; Chenna, R.; McGettigan, P. A.; McWilliam, H.; Valentin, F.; Wallace, I. M.; Wilm, A.; Lopez, R.; Thompson, J. D.; Gibson, T. J.; Higgins, D. G., Clustal W and Clustal X version 2.0. *Bioinformatics* **2007,** 23, (21), 2947-8.
62. Zimmermann, L.; Stephens, A.; Nam, S. Z.; Rau, D.; Kübler, J.; Lozajic, M.; Gabler, F.; Söding, J.; Lupas, A. N.; Alva, V., A Completely Reimplemented MPI Bioinformatics Toolkit with a New HHpred Server at its Core. *J Mol Biol* **2018,** 430, (15), 2237-2243.
63. Trifinopoulos, J.; Nguyen, L. T.; von Haeseler, A.; Minh, B. Q., W-IQ-TREE: a fast online phylogenetic tool for maximum likelihood analysis. *Nucleic Acids Res* **2016,** 44, (W1), W232-5.
64. Le, S. Q.; Lartillot, N.; Gascuel, O., Phylogenetic mixture models for proteins. *Philos Trans R Soc Lond B Biol Sci* **2008,** 363, (1512), 3965-76.